LUND UNIVERSITY

Master Thesis

Dimples in corrugated channels to improve efficiency in plate heat exchangers

by

Gustav Karlsson

Department of Chemical Engineering
Lund University
Sweden
June 25, 2020

Supervisor: **Doctor Niklas Andersson**
Examiner: **Professor Bernt Nilsson**

Front page picture: Instantaneous ray tracing illustration of heat exchanger channel.

Postal address
PO-Box 124
SE-221 00 Lund, Sweden
Web address
www.lth.se/chemeng

Visiting address
Naturvetarvägen 14

Telephone
+46 46-222 82 85
+46 46-222 00 00

Printed in Sweden by Media-Tryck.
Lund 2020

Acknowledgement

This master thesis concludes my Master of Science in Chemical Engineering at Lund University. The thesis was done for the Department of Chemical Engineering at Lund University, in collaboration with Alfa Laval Lund AB.

I would like to thank my examiner Professor Bernt Nilsson and my supervisor Niklas Andersson for assistance and inspiration throughout my master thesis.

Thanks to my supervisor at Alfa Laval, Martin Holm, for guiding me in the right direction and taking the time to teach me all things CFD-related. Thank you to Erik Engström and Matz Andersson for accompanying me at the Alfa Laval head office and keeping my head up during the last couple of months, when most people were working from home due to the Coronavirus pandemic.

Also, thank you to the colleagues at the GPHE R&D-department at Alfa Laval for welcoming me with open arms and sharing many laughs together in the break room. I learned many things from you, not least the importance of team spirit and having fun at your workplace.

Finally, i would like to give a special thanks and gratitude to Professor Christer Fureby for excellent mentorship and assistance in the project. Your deep knowledge and expertise has pushed this thesis to much more than what I thought was possible! It would not have been the same without you.

Thank You!

Gustav Karlsson
2020-05-29, Lund

Abstract

The development of new heat exchanger patterns is ever changing. Companies are constantly pushing innovation to satisfy costumer needs in terms of thermal efficiency, reliability and serviceability. In this thesis, the implementation of dimples in the corrugated pattern of a plate heat exchanger is investigated to increase thermal efficiency.

The thesis comprises three studies, moving from research of a dimpled surface to implementation of dimples on a real-life heat exchanger model used by Alfa Laval. Computational fluid dynamics was applied to model heat transfer, pressure drop and thermal efficiency through three Reynolds Averaged Navier Stokes (RANS) models and one Large Eddy Simulation (LES). The RANS-models were shown to provide insufficient resolution which heavily affected mixing, vortex formation and flow distribution in the heat exchanger channel. The RANS-model suggested that the thermal efficiency decreases when dimples are added, but failed to accurately capture key phenomena such as vortex formation and mixing. In the more advanced LES model, dimples were shown to increase the thermal efficiency by 18 % compared to a flat channel.

This study not only provides insight into the flow behavior in dimpled heat exchanger channels, but also shows the importance of using the correct turbulence model for a given problem. The flow dynamics in a dimpled plate heat exchanger is complex, and a RANS-model is not sufficient for an accurate description of the velocity field. In this regard, LES performs better and the result of the LES simulation is therefore more trustworthy than results from the RANS. As no experimental data exists, it is difficult to compare models to reality, laboratory trials are nessessary.

Sammanfattning

Värmeväxlare och värmeväxlarmönster utvecklas ständigt. Företag driver innovationen framåt för att hela tiden utveckla nya värmeväxlarprodukter för att tillfredställa sina kunders krav på termisk effektivitet, tillförlitlighet och brukbarhet. I denna avhandling behandlas användningen av dimplar i värmeytan av plattvärmeväxlare för att öka den termiska effektiviteten.

Avhandlingen består av tre studier, från studier av raka dimplade ytor till implementation av dimplar i en model av en värmeväxlarprodukt som används av Alfa Laval. Datorbaserad flödessimulering användes för att beskriva flödesdynamiken och resultaten utvärderades genom värmeöverföring, tryckfall och termisk effektivitet. För att beskriva turbulensen användes två modeller, en Reynolds Averaged Navier Stokes (RANS) och en Large Eddy Simulation (LES). RANS-modellen visade sig prestera svagt, med otillräcklig upplösning av flödesstukturer vilket påverkade omblandning, vortex-bildning och flödesfördelning i värmeväxlarkanalen. RANS-modelen antydde att den termiska effektiviteten minskade när dimplar användes, men misslyckades med att fånga fenomen såsom vortex-bildning och omblandning. I den mer avancerade LES-modelen, ökade dimplar den termiska effektiviteten med 18 % jämfört med en kanal utan dimplar.

Denna avhandling ger inte bara insikt i hur flödet beter sig i en dimplad värmeväxlarkanal, utan visar också vikten av att använda rätt turbulensmodel för ett givet problem. Flödet i en värmeväxlarkanal är mycket dynamiskt och svårt att beskriva, vilket gör att RANS-modellen är otillräcklig för exakt beskrivning av hastighetsfältet. I denna bemärkelse presterar LES bättre vilket gör att resultaten är mer tillförliga för LES än RANS. Då ingen experimentell data existerar, är det svårt att jämföra modellerna med verkligheten, för detta behövs labtester göras.

Popular science summary

Plate heat exchangers find their main use as a heat recovery unit in refrigeration, petrochemical plants, pulp and paper, pharmaceutical production, food industry and waste water treatment. Energy and utilities are of great importance in today's world, as companies shift towards reduced carbon emissions and minimizing water and energy consumption to protect the environment. The energy saving capability of a plate heat exchanger is dictated by the corrugated pattern, as this is where most of the heat transfer occurs.

New plate heat exchanger products are constantly developed to satisfy costumer needs in terms of thermal efficiency, reliability and serviceability. A heat transfer enhancement technique used to improve thermal efficiency through mixing, is the addition of dimples. Dimples are commonly used today, on aeroplane wings to reduce fuel consumption and on the surface of golf balls to increase travel distance. Dimples in corrugated plate heat exchanger channels is an area that has not yet been explored sufficiently, but recent advancements in the field has sparked the interest of an investigation.

The implementation of dimples on a corrugated heat exchanger pattern through a computational fluid dynamic model was performed in Ansys CFX, which revealed formation of vortex structures emanating from the dimple cavities. The dimples were shown to enhance mixing, vortex formation and provide beneficial flow distribution in the model of the plate heat exchanger channel. The results also included state of the art fluid dynamics simulations with conclusions about the insufficiency of certain models in regards to mixing and vortex formation.

Through this research, an increased understanding of dimples in plate heat exchangers has been achieved which can contribute to better products with higher thermal efficiency. In the future, the next generation of heat exchangers will continue to contribute to save reduced energy consumption, possibly with the addition of dimples.

Populärvetenskaplig sammanfattning

Plattvärmeväxlare används för att återvinna värme och återfinns i så gott som alla industribranscher. Exempel på områden där värmeväxlare används är vattenrening, petrokemi, läkemedelsindustrin samt pappers- och massaindustrin. Effektivt användade av energi och vatten är av stor vikt i dagens samhälle, när både företag och individer siktar mot reducerade kolutsläpp och minimerad vatten- och energianvändning för att skydda miljön. En plattvärmeväxlares energibesparingsförmåga bestäms av värmeytan, där majoriteten av värmeöverföringen sker.

Nya plattvärmeväxlare utvecklas ständigt för att tillfredställa kunders behov av termisk effektivitet, tillförlitlighet och brukbarhet. En teknik som används för att förstärka värmeöverföringen genom ökad omblanding är användandet av dimplar. Dimplar har idag många användingsområden, som i flygplansvingar för att minska bränslekonsumption och i golfbollar för att de ska flyga längre. Användningen av dimplar i värmeytan av plattvärmeväxlare har inte undersökts tillräckligt, men nya framsteg inom området har väckt intresset för en undersökning.

Dimplar har implementerats i värmeytan av en plattvärmeväxlare genom en datorbaserad flödesdynamiksmodel i Ansys CFX, vilket visade formationer av vortexar bildade i dimplarnas hålrum. Dimplarna visade sig förbättra omblandning, vortexbildning och bidra med fördelaktig flödesfördelning i plattvärmeväxlarens kanal. Resultaten inkluderar framstående flödesdynamiska simuleringar med slutsatser angående otillräckligheten av vissa modeler baserat på omblandning och vortexbildning.

Denna avhandling ger ökad förståelse för dimplar i plattvärmeväxlarkanaler, vilket kan bidra till bättre produkter med högre termisk effektivitet. I framtiden kommer nästa generations värmeväxlare fortsätta reducera energikonsumptionen, möjligen med användningen av dimplar.

Nomenclature

α	Area average convective heat transfer coefficient, [J/(m^2K)]
β	Corrugation angle, [°]
Δp	Total pressure loss from inlet to outlet, [Pa]
ΔT_L	Logaritmic mean temperature between heating wall and bulk of the flow, [K]
ϵ	Rate of dissipation of turbulent kinetic energy
η	Thermal efficiency, [-]
λ	Thermal conductivity, [W/(m k)]
$\langle u_i u_j \rangle$	Reynolds Stress
µ	Dynamic viscosity, [Pa s]
ν	Kinematic viscosity, [m$^2/s$]
ω	frequency
$\overline{v}$	Average velocity, [m/s]
ρ	Density, [kg/m^3]
A_{HS}	Heat transfer area of channel wall, [m^2]
C_f	Fanning friction factor, [-]
D_h	Hydraulic diameter, [m]
DNS	Direct Numerical Simulation
k	Turbulent kinetic energy
L	Length of heat exchanger channel, [m]
LES	Large Eddy Simulation

Nu Average Nusselt number, [-]

Q Heat flux over channel wall, [W]

$RANS$ Reynolds Averaged Navier-Stokes

Re Reynolds number, [-]

RMS Root Square Mean

T_W Temperature at channel wall, [K]

T_{in} Temperature at inlet, [K]

T_{out} Temperature at outlet, [K]

u_r Friction velocity, [m/s]

v Velocity, [m/s]

y Absolute distance to wall, [m]

y^+ Absolute distance from wall in wall units, [-]

Contents

1 Introduction **1**
1.1 Overview . . . 1
1.2 Aim and Project Scope . . . 2

2 Background **3**
2.1 Transport in Plate Heat exchangers . . . 3
2.1.1 Operation . . . 4
2.1.2 Governing equations . . . 5
2.2 Computational Fluid Dynamics Modeling . . . 7
2.2.1 Geometric Domain and Meshing . . . 8
2.2.2 Physics . . . 8
2.2.3 Solver setup . . . 9
2.2.4 Post Processing . . . 10
2.2.5 Mathematics in CFD . . . 11
2.3 Dimple applications . . . 15

3 Materials and Methods **16**
3.1 Setup-Guide . . . 17
3.2 Flow structure on Dimpled Surfaces . . . 20
3.2.1 Arrangement . . . 22
3.2.2 Reynolds sweep . . . 22
3.3 Singular Heat exchanger Channel . . . 23
3.3.1 Position . . . 25
3.3.2 Near wall meshing sensitivity . . . 27
3.4 Herringbone Pattern . . . 29
3.4.1 Implementation of Dimples . . . 31

4 Result and Discussion **34**
4.1 Flow structure on Dimpled Surfaces . . . 34
4.1.1 Arrangement . . . 34
4.1.2 Reynolds Sweep . . . 39
4.2 Singular Heat exchanger Channel . . . 42
4.2.1 Position . . . 42
4.2.2 Near wall mesh sensitivity . . . 44
4.3 HerringBone Pattern . . . 46
4.3.1 Implementation of dimples . . . 46
4.4 LES simulation . . . 51

5 Conclusion **55**

6 Future Work **56**

References **57**

A Appendix **58**
A.1 Finite Volume Method 58
A.2 Fourier transform - Pressure drop 61
A.3 Fourier transform - Temperature 62
A.4 Fourier transform - Velocity 63

1 Introduction

1.1 Overview

The development of new heat exchanger patterns is ever changing. New products are constantly developed to satisfy costumer needs in terms of thermal efficiency, reliability and serviceability. To increase the thermal efficiency of a heat exchanger, the corrugated pattern is often an area of great focus, as this is where most of the heat transfer occurs (Alfa Laval Corporate AB. 2020). The usage of dimples in corrugated plate heat exchanger patterns is an area that has not yet been explored sufficiently, but recent scientific articles has sparked the interest of an investigation.

(Ferhat et al. 2019) introduces a concept of "artificial roughness" to improve the heat transfer within corrugated channels. The goal of the paper was to investigate artificial roughness and how it affects the performance of plate heat exchangers. The results show a 50 % increase in thermal performance by using artificial roughness and added undulations compared to a flat channel. Several other studies have been conducted, also showing promising results (Chudnovsky and Kozlov 2006) (Elyyan 2008).

Alfa Laval is now interested in preforming their own study, confirming the findings in the article by Ferhat, and investigating the usage of micropatterns in the form of adding dimples to a corrugated heat exchanger channel.

This master thesis will be divided into three parts, with each part contributing to the overall investigation of dimpled micropatterns in plate heat exchangers. The parts will mirror the workflow of the project, starting with a general investigation of dimpled surfaces and ending with the implementation of dimples on the corrugated pattern of a model that is currently used by Alfa Laval.

1.2 Aim and Project Scope

The aim of this master thesis is to investigate if dimpled geometries can increase the performance of plate heat exchangers. This will be done by developing a new corrugated pattern using dimples on a current product used at Alfa Laval. A secondary objective of this thesis will be to increase the understanding of flow structures located within corrugated heat exchanger channels and their contribution to heat transfer and pressure loss.

The scope of the master thesis follows that outlines the elements that are inside and outside the scope of this project. The project scope is summarized in the Table below.

In Scope	Out of Scope
- Design of a new and improved corrugated GPHE pattern by modification of an existing geometric model using dimples with the goal of maximizing heat transfer while minimizing pressure drop.	- Validation and calibration of simulation results based on experimental data.
- Development of a high resolution simulation model using Computational fluid dynamic software ANSYS CFX for quantitative and visual analysis of dimpled heat exchanger channels.	- Economic cost calculation of implementing dimples compared to a standard corrugated pattern.
- Perform a numerical analysis that compares simulations with- and without dimples to evaluate performance based on heat transfer, pressure drop and thermal efficiency.	- Investigation of conjugate heat transfer ie the transfer of heat between a hot and cold fluid separated in two different channels.
- Produce three cases that investigates flow structure on dimples surfaces, investigation of a singular heat exchanger channel and implementation on a herring bone pattern.	

2 Background

2.1 Transport in Plate Heat exchangers

Plate heat exchangers (PHE) find their main applications in liquid-liquid duties where high heat transfer is of importance. They are most commonly used in the food industry such as dairy and beverage processing but also find use in paper mills, petrochemical plants, closed-circuit cooling systems and process heaters. The ability to remove, replace and clean individual plates and the separation of fluids by a physical wall makes the PHE ideal for sterile processing such as pasteurization.
One of the the major advantages of the PHE compared to the shell-and-tube heat exchanger is its flexibility. Individual plates can be taken out and changed to fit a different task through plate size, corrugation pattern and arrangement.
The heat transfer coefficient is much larger for a PHE compared to a shell-and-tube heat exchanger, which makes the required surface area about 1/3 for a given heat duty. This means that the PHE takes up much less space compared to a shell-and-tube heat exchanger, which can be an important factor as customers value space inside their factories (Shah, Subbarao, and Mashelkar 1986).

2.1.1 Operation

The plate heat exchanger consists of a number of rectangular plates held together with a frame. Each plate is pressed with a corrugated surface pattern on a piece of sheet metal. The corrugated plates are mounted successively as to form passages between the plates to guide the flow of media from one end to the other (Shah, Subbarao, and Mashelkar 1986). A plate heat exchanger together with a corrugated pattern is shown in Figure 2.1.

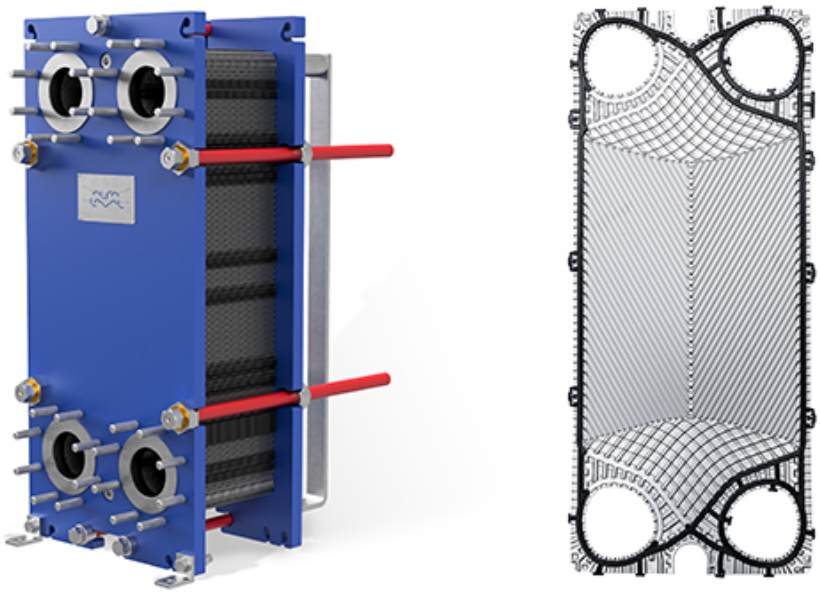

Figure 2.1 – An example of a PHE from Alfa Laval (left) and a corrugated plate (right).

The corrugated pattern provides mechanical support through multiple contact points as well as enhances the heat transfer by increasing the level of turbulence. There are many different plate patterns available today, one of which is the Herringbone design. The Herringbone design consists of corrugated plates inclined at an angle β to the flow direction. The assembly is done with every other plate pointing in the opposite direction, creating narrow flow passages. A figure of a herring bone pattern with an illustration of a flow passage is shown in Figure 2.2.

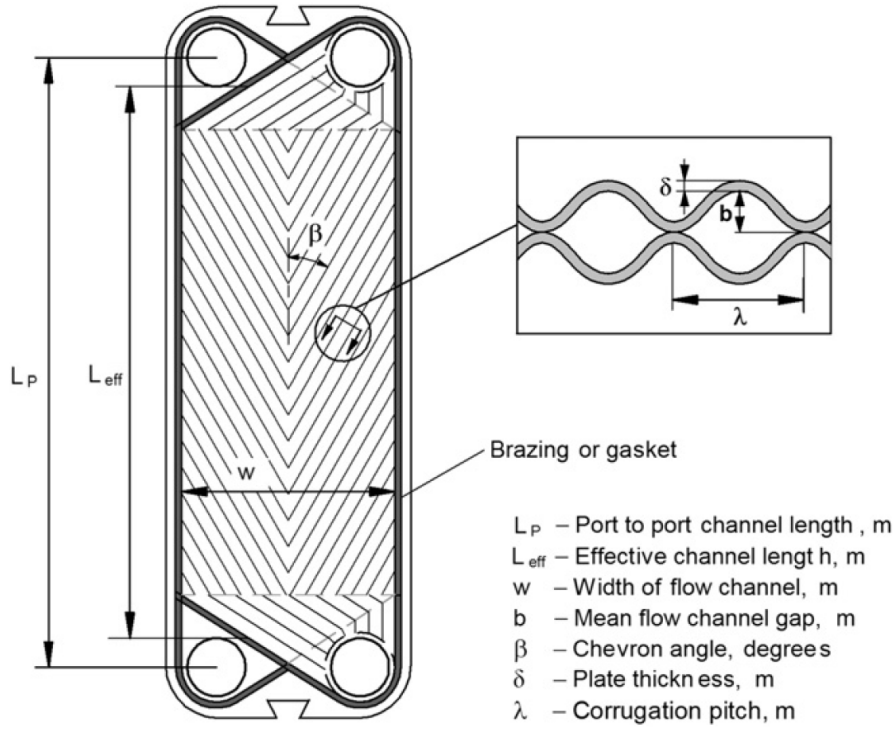

Figure 2.2 – Herringbone pattern with corrugation angle β and illustration of flow channel geometry.

Several known mechanisms contribute to the high heat transfer coefficient inside PHEs. Any design containing protrusions and intrusions will cause boundary layer separation and reattachment which leads to earlier transition to turbulent flow. This will lead to enhanced heat transfer but with the cost of increased pressure drop. In herringbone design, the crisscrossing nature of the corrugations produces swirl flows which enhance mixing. This is one of the reasons that the herringbone pattern is generally superior to other designs in terms of heat transfer over friction and is the most commonly used design today (Shah, Subbarao, and Mashelkar 1986).

2.1.2 Governing equations

The area average convective heat transfer coefficient of the heat exchanger channel is defined by

$$\alpha = \frac{Q}{A_{HS}\Delta T_L} \tag{2.1}$$

where Q is the heat flux over the channel wall and A_{HS} is the area of the channel wall. ΔT_L is the log mean temperature difference between the heating wall and the

bulk of the flow and is described by equation 2.2, where T_w is the temperature at the channel wall.

$$\Delta T_L = \frac{(T_w - T_{in}) - (T_w - T_{out})}{ln(\frac{T_w - T_{in}}{T_w - T_{out}})} \tag{2.2}$$

The average Nusselt number is defined by:

$$Nu = \frac{\alpha D_h}{\lambda} \tag{2.3}$$

Where α is the area averaged convective heat transfer coefficient, D_h is the hydraulic diameter and λ is the thermal conductivity of the fluid.

The Reynolds number is defined as

$$Re = \frac{D_h \overline{v} \rho}{\mu} \tag{2.4}$$

where $\overline{u}$ is the average velocity inside the channel, ρ is the density of the fluid and μ is the dynamic viscosity.

The pressure drop inside the channel is described by Fanning friction factor calculated as

$$C_f = \frac{\Delta p}{4} \frac{D_H}{L} \frac{2}{\rho \overline{u}^2} \tag{2.5}$$

where Δp is the total pressure loss from inlet to outlet and L is the length of the channel.

The thermal efficiency of a heat exchanger channel is defined as

$$\eta = \frac{Nu}{C_f^{1/3}} \tag{2.6}$$

2.2 Computational Fluid Dynamics Modeling

Computational Fluid Dynamics (CFD) is a branch of fluid mechanics that uses computer based simulations to model the behavior of systems involving fluid flow, heat transfer and other physical phenomena. It operates by solving numerical equations of fluid flow with specified conditions on the boundary of a region.

Recent advances in computer power allowed CFD modeling to move from being a tool almost extensively used in research to being an established industrial design tool. Powerful computers have made the process of creating models and analyzing results much less labor intensive which reduces time and the therefore also cost. CFD has proved to be a cost effective and accurate alternative to laboratory testing with the ability to skip manufacturing test rigs and make alterations on the fly (Ansys Inc. 2020).

The process of performing a CFD simulation can be split into four components: geometric domain and meshing, physics, solver setup and post processing. The following sections will describe each component.

2.2.1 Geometric Domain and Meshing

Creating a geometric domain is the first step in preforming a CFD simulation. Defining a geometry of the region of interest needs to be done before any other component can be considered. Often, the geometry can be imported from any CAD software.

The geometric domain is divided into smaller subregions, in a gridlike structure called a mesh. A single cell inside the grid network is called an element. A high resolution mesh contains a large amount of elements and requires a significant computational effort, while a low resolution mesh contains a small amount of elements and processes quickly. Both high and low resolution meshes have their uses depending on the complexity of the problem. The elements can have different shapes: hexahedral, rectangular, prism, tetrahedral or polyhedral and influence the numerical convergence by communicating amongst each other. Figure 2.3 describes the conversion of a geometric domain into a mesh.

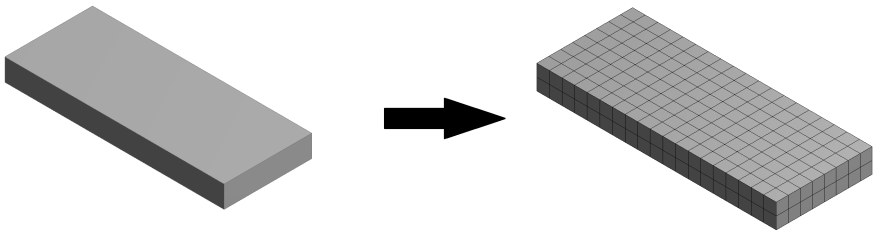

Figure 2.3 – Illustrative example of going from a geometric domain to implementing a mesh.

2.2.2 Physics

After the geometry is specified, some assumptions have to be made regarding the physics of the simulation. These include the selection of fluid properties, boundary conditions and initial conditions. Fluid properties include the choice of materials such as continuous fluid or dispersed particles as well as selecting the turbulence model. Boundary conditions include specifying the boundaries of the domain such as inlet and outlet and the assumptions made at these boundaries such as temperature, velocity and pressure. Initial conditions cover the global properties that apply within the domain at the start of the simulation.

2.2.3 Solver setup

The component that solves the CFD problem is called the solver. The solver operates by integrating partial differential equations over all elements inside the domain. The integral equations are converted to a system of algebraic equations which are being solved iteratively through a Finite Volume method described in Appendix A.1. As the solver moves through the iterations it approaches an exact solution, it converges. After each iteration, a residual, or error, is reported to measure the overall conservation of flow properties. A small residual indicates a well converged solution.

There are two types of solution procedures: steady state and transient. These will be briefly described in the sections below.

Steady state: A steady state simulation is a solution procedure where the system or process are unchanging in time. Flows that do not change over time requires only one solution and reaching convergence to this solution is therefore the objective. The solution procedure uses loops to iterate over flow equations and approach a final solution. The solver will stop iterating after a convergence criteria is reached.

Transient: A transient simulation is a solution procedure with the objective of studying change over time. Transient simulation in CFD uses time steps to divide the total simulation time into intervals. The fluid is allowed to flow during a time step and partial differential equations are solved for that realization of the flow. The next time step is initialized and this process is repeated until the total simulation time is reached (Wikipedia The Free Encyclopedia. 2020). Figure 2.4 shows a transient solution setup.

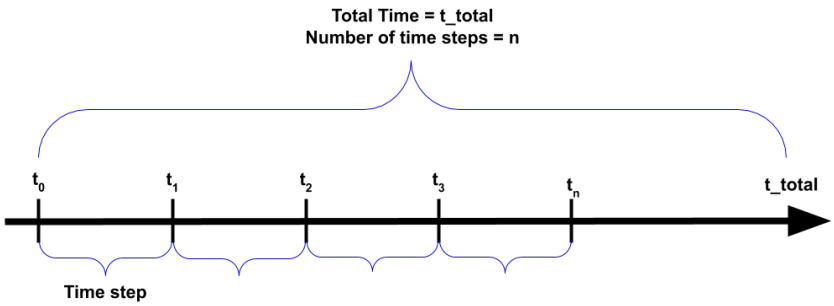

Figure 2.4 – Illustrative example of a Transient solution setup.

2.2.4 Post Processing

The post processing component is used to visualize and analyze the results produced by the solver in an intuitive manner. Visualization of scalar variables such as temperature, pressure and velocity is a major use of the post processing software. The user can also interact with the post processing software to create animated sequences, quantitative numerical calculations as well as vector and contour plots through the domain.

2.2.5 Mathematics in CFD

Mathematics in CFD is based on a set of equations to describe the processes of momentum and mass transfer, known as Navier-Stokes equations. Navier-Stokes are partial differential equations and is also called the *momentum equation*. It technically only describes the motion of a viscous fluid, however when the momentum equation is complemented with the *continuity equation* for mass conversation, they provide a complete mathematical description of a viscous fluid. Usually, the term Navier-Stokes equations is used to refer to both of these equations, not only the momentum equation. The continuity equation and the momentum equation are presented in 2.7 and 2.8 respectively.

$$\frac{\partial \rho}{\partial t} + \rho(\nabla \boldsymbol{v}) = 0 \tag{2.7}$$

$$\rho \left(\frac{\partial \boldsymbol{v}}{\partial t} + \boldsymbol{v} \cdot \nabla \boldsymbol{v} \right) = -\nabla P + \mu \nabla^2 \boldsymbol{v} + \boldsymbol{\rho g} \tag{2.8}$$

The momentum equation can also be expressed in Lagrangian form, which can be seen in equation 2.9.

$$\rho \frac{D\boldsymbol{v}}{Dt} = \mu \frac{\partial^2 \boldsymbol{v}}{\partial x_i \partial x_i} - \frac{\partial P}{\partial x_j} - \rho \frac{\partial g}{\partial x_j} \tag{2.9}$$

Navier-Stokes equations have no general analytical solution, but can be discretized and solved numerically (Ansys Inc. 2020). Discretization is based on solving equations at discrete points instead of general solutions, illustrated in Figure A.1.

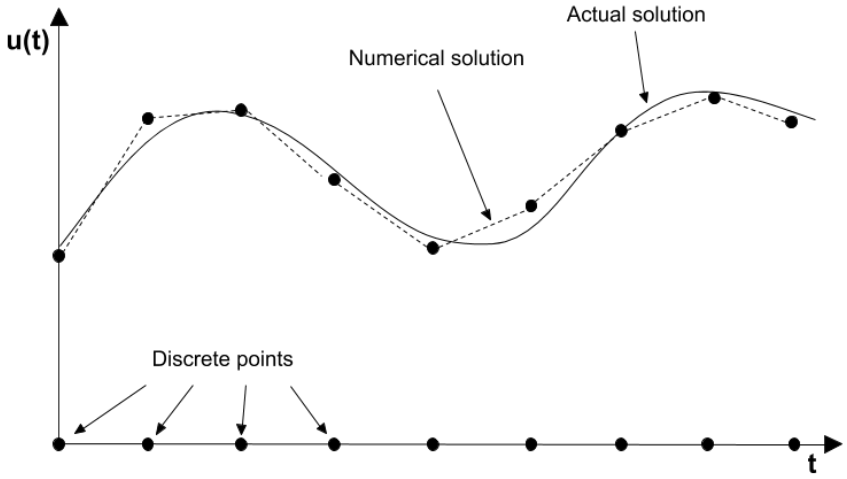

Figure 2.5 – Illustration of an general solution of an equation (straight line) and a numerical solution at discrete points (dashed line).

There are several techniques for numerical solutions of Navier-Stokes equations, some of which are Direct Numerical Simulation (DNS), Large Eddy Simulation (LES) and Reynolds Averaged Navier-Stokes (RANS). These techniques are presented below.

Direct Numerical Simulation

Direct Numerical Simulation (DNS) consist of solving the Navier-Stokes equations to determine the instantaneous velocity field *v(x,t)* for one realization of the flow. This involves resolving all time- and lengthscales, down to the the smallest scales of motion. Resolution of the smallest dissipative motions require a grid spacing small enough to capture the fully developed turbulent structure, which often requires 10^9 cells.

Conceptually, DNS is the simplest of the modeling approaches as it involves straightforward solution of the Navier-Stokes equations. Visualization can be performed to examine turbulent structures with complete accuracy and unrivaled level of description compared to other models available. However, the computational cost is extremely high and increases drastically with Reynolds number, leaving DNS to be applicable only to flows of low or moderate Reynolds numbers. Performing a DNS simulation is a time consuming affair, even on powerful supercomputers with 10^3 cores. In most engineering applications, the objective of determining mean velocity in turbulent flow mismatches the DNS approach, as 99% of the computational effort devoted to the dissipation range. The DNS approach was infeasible until the 1970s when computers of sufficient power became available. Today, it is mainly used in special research applications. (Pope 2000)

Large Eddy Simulation

Like DNS, the Large Eddy Simulation (LES) operates by obtaining a time-dependent velocity field, $v(x,t)$, that represents the velocity field for one realization of turbulent flow. However the time-dependent velocity field is "filtered" to represent only larger-scale turbulent motions, while smaller-scale motions are solved using a simple model. The low-pass filtering operation is defined by equation 2.10.

$$\overline{\boldsymbol{v}}(x,t) = \int G(r,x)\boldsymbol{v}(x-r,t)dr \tag{2.10}$$

Where integration is over the entire domain, $\overline{v}$(x,t) is the filtered velocity field and G is the specificed filtering function. The residual field is defined by

$$\boldsymbol{v'}(x,t) \equiv \boldsymbol{v}(x,t) - \overline{\boldsymbol{v}}(x,t) \tag{2.11}$$

So that the velocity field has the decomposition

$$\boldsymbol{v}(x,t) = \overline{\boldsymbol{v}}(x,t) + \boldsymbol{v'}(x,t) \tag{2.12}$$

This may appear equivalent to Reynolds Decomposition, but an important difference is that $\overline{v}$(x,t) is a random, fluctuating field and therefore has a non-zero residual.

$$\overline{\boldsymbol{v'}}(x,t) \neq 0 \tag{2.13}$$

As described in the section above, the computational cost of DNS is high and only applicable to low or moderate Reynolds numbers. LES is motivated by this limitation, as the computational effort of DNS is expended at the smallest motions, whereas the majority of the energy is located in the larger scales of motion. Thus, LES avoids the vast computational effort of DNS while capturing a large majority of the dissipative energy range. The level of description in LES is more than sufficient for most applications. Because the velocity field is filtered, some approximations are involved but in practice this is not a major concern. Compared to RANS, LES has the advantage of capturing the unsteady, large-scale turbulent structures and can therefore be used to study aerodynamics and acoustics or other phenomena associated with unsteady turbulent motions. (Pope 2000)

Reynolds Averaged Navier-Stokes

In contrast to DNS and LES, RANS does not solve time-dependent velocity fields. Instead, the RANS approach uses turbulence models to determine the mean velocity $\langle \boldsymbol{v} \rangle$ from Reynolds equations, that can be seen in equation 2.14.

$$\rho \frac{D\langle \boldsymbol{v} \rangle}{Dt} = \mu \frac{\partial^2 \langle \boldsymbol{v} \rangle}{\partial x_i \partial x_i} - \frac{\partial \langle P \rangle}{\partial x_j} - \rho \frac{\partial \langle g \rangle}{\partial x_j} - \rho \frac{\partial \langle u_i u_j \rangle}{\partial x_j} \tag{2.14}$$

Reynolds equations are very similar to Navier-Stokes equations (see equation 2.9) except for the substitution of the instantaneous velocity field $\boldsymbol{v}$ for the mean velocity field $\langle v \rangle$ and the addition of the term $\langle u_i u_j \rangle$, which describe the Reynolds stress. The way in which the RANS models determines $\langle u_i u_j \rangle$ is what defines the RANS models.

There are several models available and most of them can be divided into two categories: Turbulent-viscosity models and Reynolds-stress models. Turbulent viscosity models obtain the Reynolds stress from turbulent viscosity, which in turn is described either algebraically or from turbulent quantities such as k, ε and ω for which two-equation models are solved. In Reynolds-stress models, transport modelled equations are solved for Reynolds stresses directly, and therefore eliminating the need for a turbulent viscosity (Pope 2000). Figure 2.6 shows an illustration of the different RANS models and how they fit together.

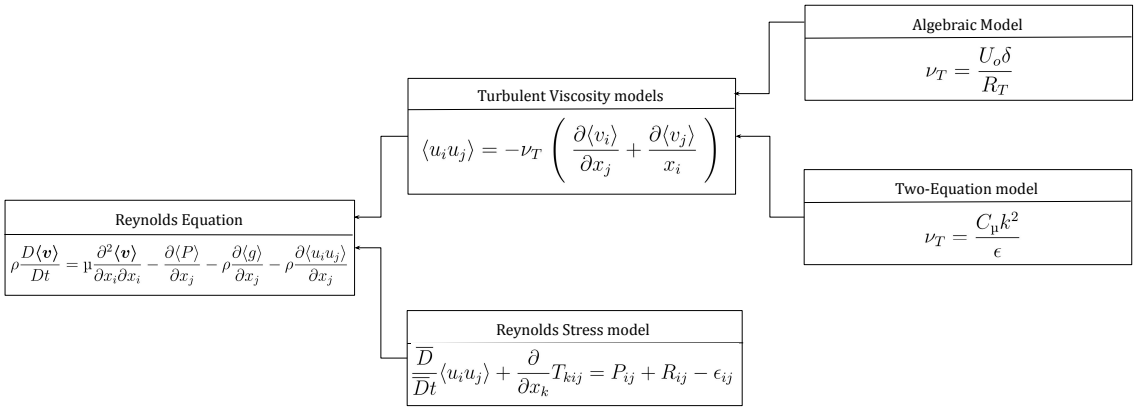

Figure 2.6 – Illustration of RANS-models decomposition into Algebraic models, Two-equation models and Reynold-Stress models.

2.3 Dimple applications

Dimples has its use in many applications such as golf balls and aeroplane wings. A central concept when discussing the effect of dimples is boundary layer separation. A body immersed in a flow of fluid creates a thin boundary layer adjacent to the solid body. In the boundary layer, velocity varies from zero close to the wall to the free stream velocity in the bulk flow. The fluid layer adjacent to the solid wall has to overcome surface friction which at some points causes the flow to separate from the body. This point is called the point of separation. The point of separation can be delayed by using dimples to transition from laminar to turbulent boundary layer, which is an effect seen in golf balls. Figure 2.7 shows an illustration of a golf ball with dimples, delaying the point of separation.

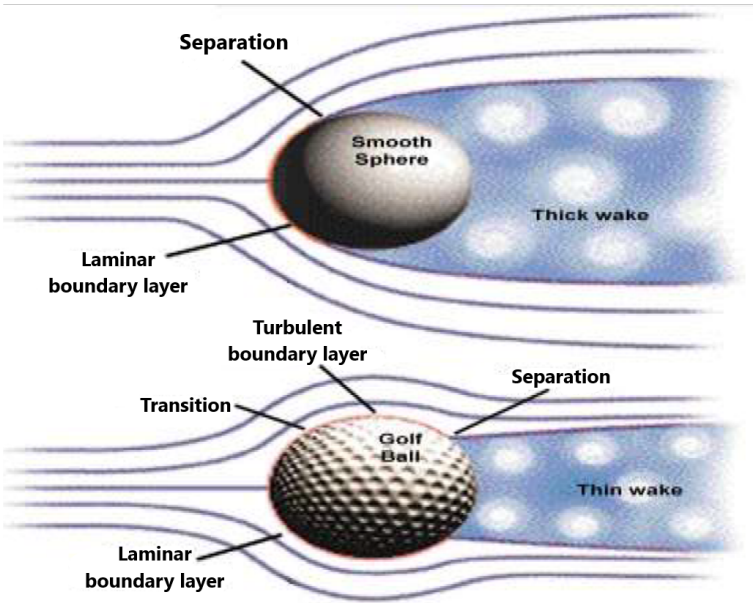

Figure 2.7 – Illustrative example of boundary layer separation in a golf ball.

As is illustrated in Figure 2.7, the transition to turbulent flow allows the boundary layer to stay attached to the ball much longer which produces smaller low pressure wakes behind the ball. The reduction in pressure drag causes the ball to travel further than without dimples (Livya, Anitha, and Valli 2015).

Dimples on an aeroplane wing show similar functionality. Generation of vortexes in the dimple cavity help delay the boundary later separation. The vortexes push the boundary layer from laminar to turbulent which causes the boundary layer to stay attached for longer (Prasath and Angelin 2017).

3 Materials and Methods

The material part of this report consists of a setup-guide and three case studies. In the setup guide mutual information that is valid throughout case 1, 2 and 3 will be presented such as creation of dimples, meshing strategy and setup of the numerical solver in ANSYS CFX 2019 R3, whereafter this terminology will be applied to ALL three cases. Note that the first part of the methods section applies to all three cases, but with some modification due to differences between the cases. This is done partly to save space in the report, but also due to convenience for the reader.

After the shared part is described, each case will be presented including its specific methodologies and specifications. The cases are:

1. Flow structures on dimpled surfaces
2. Investigation of a singular heat exchanger channel
3. Implementation on of dimples on a herringbone plate pattern

The cases mirror the workflow of the project and goes from idea and overall observations of dimpled geometries in Case 1, to a complete implementation of a dimpled pattern into a real life model of plate heat exchanger in Case 3.

Each case will contribute towards the overall recommendation for an implementation of a dimpled pattern to be used in Alfa Lavals heat exchanger.

3.1 Setup-Guide

This part will contain a setup-guide that describes a general methodology which is used in case 1, 2 and 3. The goal is to collect information that is valid throughout the cases under a single heading, so that repetition is minimized.

The geometric domain is different for each case, but with some similarities. In general, the dimensions of the domain is small compared to the size of a heat exchanger plate. This is done intentionally to allow increased meshing resolution while keeping computational effort at a minimum. A high meshing resolution is important to resolve flow structures around the dimples at a sufficient level. Numeric quantities obtained from the simulation can be extrapolated to fit the size of a real heat exchanger product.

The spherical dimple geometry considered in this report were developed with guidance from previous studies from (Turnow, Zhdanov, and Hassel 2012) and (Banekar, Bhegade, and Sandbhor 2015), with a height-diameter ratio of 0.26. The diameter and height of each dimples was kept consistent in all cases. Two arrangements of dimples were considered, one with dimples placed in a staggered way and one with dimples placed in a line (Giram and Patil 2013). The dimple arrangements with spacing and dimensions are presented in Figure 3.1.

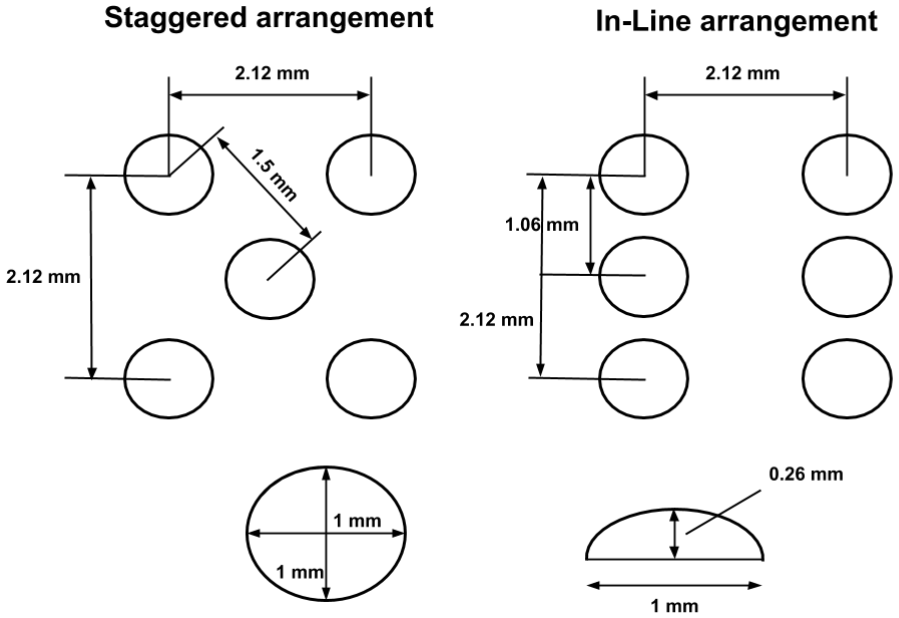

Figure 3.1 – Arrangements, spacing, height and diameter of dimples.

The mesh was done with an inflation layer. An inflation layer allows the user to create elements of increasing size connected to a surface, and is useful when there is an area of the geometry that needs a higher cell density than the rest of the domain.

The inflation layer was placed on the dimpled surface to increase the resolution around the dimples, which will resolve the thermal and turbulent boundary layers better. 10 boundary layers with a growth rate of 1.2 per layer was deemed sufficient. Figure 3.2 shows the inflation layer of a general geometric model with the red arrows showing the height of the inflation layer.

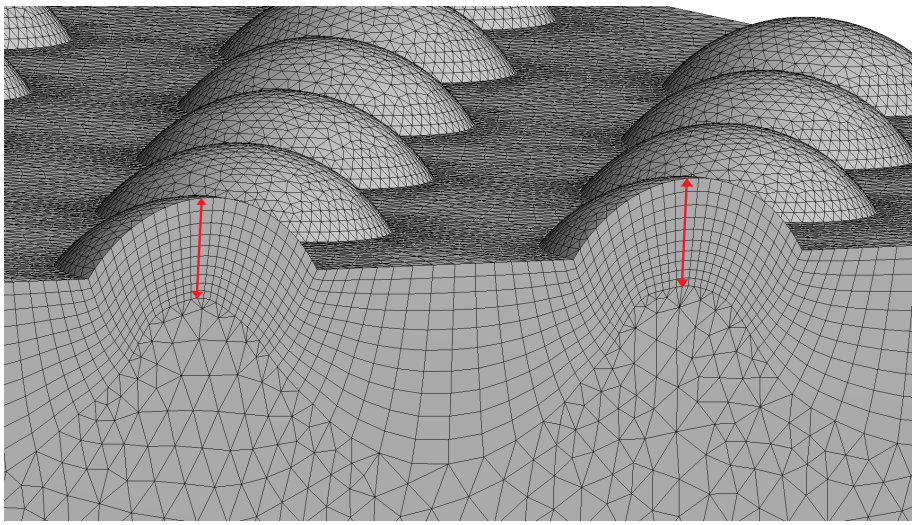

Figure 3.2 – Inflation layer mesh with a growth rate of 1.2 and red arrows indicating the height of the inflation layer.

The turbulence model is Shear Stress Transport k-ω (SST) which is a turbulent viscosity RANS-model, with automatic wall functions. The SST model is classified as a two-equation model, which means that it solves transport equations to obtain k and ω which describes the turbulent viscosity and in-turn the Reynolds Stress, see figure 2.6. SST k-ω was designed to give highly accurate predictions of flow separation which was deemed suitable for this application as detailed analysis of the flow structures in- and around the dimples is a major goal of the report. The thermal and turbulent boundary layers are affected greatly by flow separation, which is why this is an important phenomena to capture.

All boundaries are modeled as smooth no-slip walls with zero velocity next to the wall. The fluid was modeled as water without particles or droplets. Periodic boundary conditions with translational periodicity was applied to the vertical symmetric wall to reduce computational time. Figure 3.3 shows the boundaries of the model with Inlet, Outlet, Periodic Walls and Heated Walls indicated with red numbers.

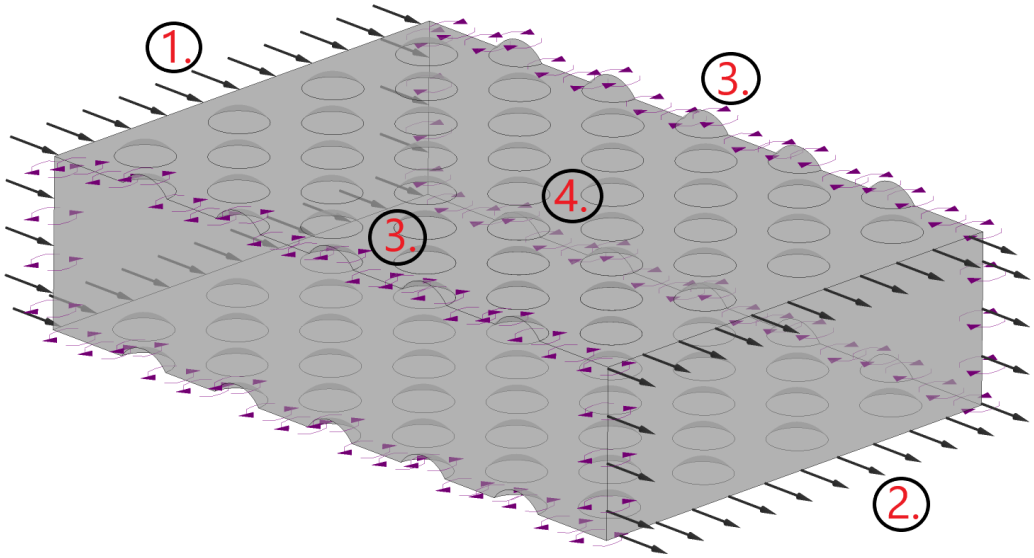

Figure 3.3 – Boundaries with the following numbering: **1.** Inlet, **2.** Outlet, **3.** Periodic Walls and **4.** Heated Walls.

The viewpoint and principle of boundary selection of Figure 3.3 with the fluid entering from the back of the geometry (1), translational periodicity along the vertical symmetric wall (3), and exiting towards the viewer (2) is valid for all cases. All figures describing geometries throughout the report can be assumed have the same principle of boundary selection as Figure 3.3.

The fluid enters the domain at atmospheric pressure and 20°C with an inlet velocity of 0.3 m/s. Heat transfer occurs on the dimpled surface on both top and bottom with a large heat transfer coefficient 20000 $W/(m^2K)$ and a constant temperature of 60°C. This is done to approach a constant wall temperature even though a heat exchanger operates through conjugate heat transfer between a cold and hot stream.

3.2 Flow structure on Dimpled Surfaces

As a prestudy to the investigation of dimples in corrugated channels, a basic research was conducted to study how a surface is affected by adding dimples. This is the first of three cases which will result in a recommendation for Alfa Lavals heat exchanger. This case will contain two sections: An arrangement study with flow structure analysis and an investigation of the dependency of Nusselts number, Fanning friction factor and thermal efficiency on Reynolds number. The arrangement study can be found in section 3.2.1 and the Reynolds study can be found in section 3.2.2.

The computational domain throughout this case is rectangular with dimples penetrating the bottom surface, and protrusions added to the top surface. The domain is 13 mm long, 8 mm wide and 3 mm high and the fluid is flowing inside the rectangular domain from one short end to the other. The geometric domain as well as dimensions is presented in Figure 3.4.

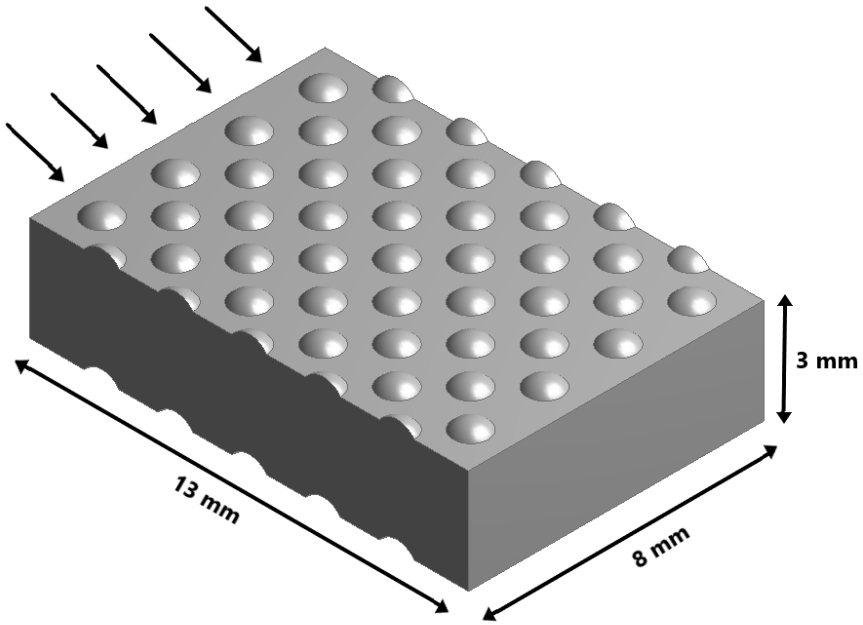

Figure 3.4 – Geometric domain for flow structure on Dimpled Surfaces with dimensions presented in the table.

As consistency between the cases was considered an important parameter, the number of dimples were kept the same between configurations. As a consequence the volume and therefore also the time of stay is equivalent between the cases, as a protrusion adds the same amount of volume as an unobtrusive dimple removes.

Including the inflation layer, the computational mesh for this case had 2.7 million elements, with 1.5 million being tetrahedral and 1.2 million being rectangular. The elements inside a single dimple was around 10000 cells. A relative quantity that can describe how well resolved a mesh is, is the cell density which has the unit [cells/volume]. The volume of the domain is 320 mm^3 and 2.7 million cells results in a total cell density of 8440 $cells/mm^3$. The computational mesh for the entire domain, including a close up of a dimple, can be seen in Figure 3.5.

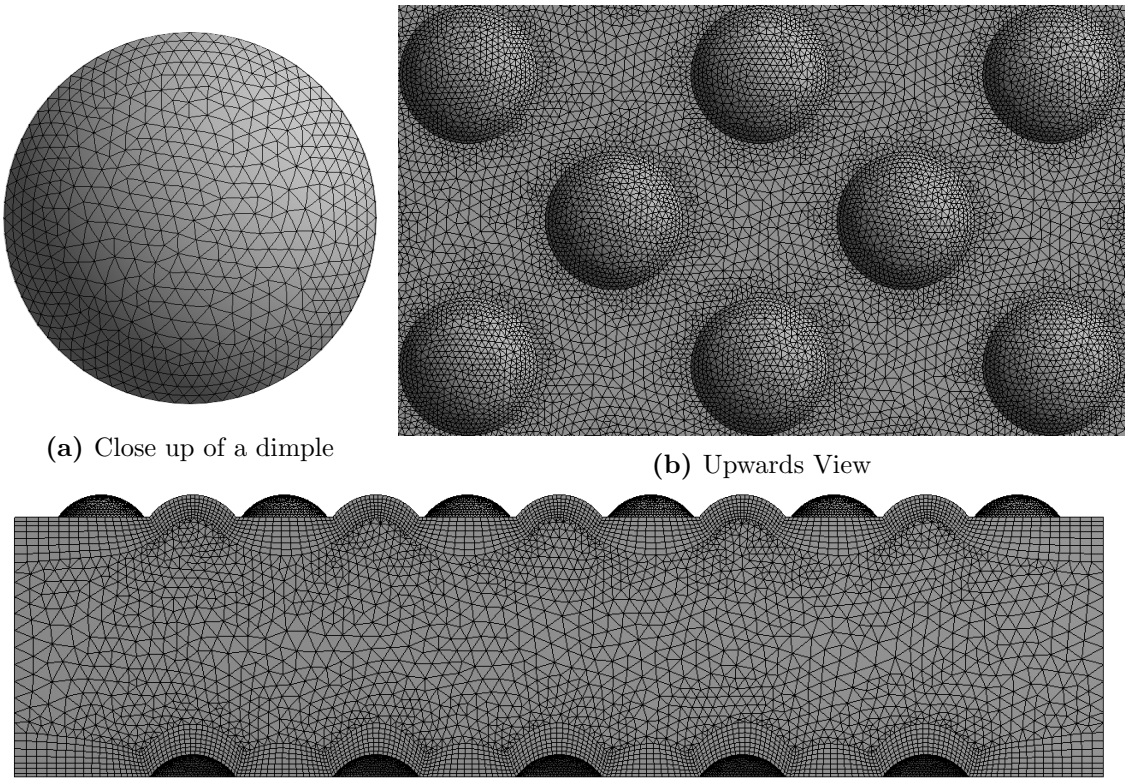

(a) Close up of a dimple

(b) Upwards View

(c) Sideways view

Figure 3.5 – Computational mesh for case study 1

The simulation type was set to Steady State. The convergence criteria was set to type Root Square Mean (RMS) with a target of 0.00005 residuals with maximum 500 iterations. Boundary condition, selection of turbulence model and meshing methodology was done according to section 3.1.

3.2.1 Arrangement

The dimples can be arranged in different configurations which will influence the secondary flow structures around each dimple. There are several arrangements to be considered but the scope was limited to two arrangements. The two dimpled configurations were staggered and in-line, which were compared to a baseline of a flat surface. The arrangements can be seen in Figure 3.6.

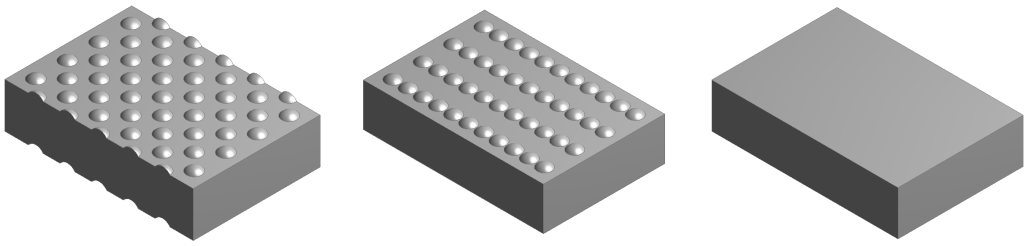

(a) Staggered **(b)** InLine **(c)** Flat

Figure 3.6 – Geometric domain for arrangement study in case 1.

The configurations will be evaluated in terms of Nusselt number for heat transfer, fanning friction factor for pressure drop and thermal effectivity coefficient for thermal effectivity.

3.2.2 Reynolds sweep

Nusselt number, Fanning friction factor and thermal efficiency is dependent on Reynolds number. To investigate this dependency, the quantities above were obtained for the staggered and flat arrangement in study 1.2.1 at different velocities. The following table shows the design points which were chosen and what quantities were measured.

Design point	Reynolds number Re [-]	Heat transfer rate Q [W]	Nusselt number Nu [-]	fanning friction factor C_f [-]	Thermal efficiency η [-]
DP 1	2000	-	-	-	-
DP 2	4000	-	-	-	-
DP 3	6000	-	-	-	-
DP 4	8000	-	-	-	-
DP 5	10000	-	-	-	-
DP 6	12000	-	-	-	-

Table 3.1 – Design points for investigating the Reynolds dependency

3.3 Singular Heat exchanger Channel

As the second out of three cases, a singlar corrugated heat exchanger channel is investigated, before implementing dimples on a herringbone pattern. A herringbone pattern would contain two plates inclined at an angle, β, with the fluid flowing in narrow passages between the plates, were as this study contains one corrugated channel without an inclination. This is a natural step towards the implementation of dimples on a herringbone pattern, as researching a singular channel will contribute to increased understanding how the flow behaves inside the corrugated channel. This is nessesary as the flow inside a herringbone pattern is irregular and chaotic, and can be difficult to interprate without investigating a singular channel first.

The geometric domain was done by extracting parts of a singular channel from a herringbone pattern and adding dimples to channel. Protruding dimples were added to the top the channel, penetrating into the channel and obtrusions were added to the bottom. Equivalent to section 3.2, the same number of dimples were added on top and bottom to ensure that the volume is kept constant. The fluid is flowing through the channel, from back to front. The rectangular extention at the front of the geometry was added to ensure that backflow was minimized by allowing the flow profile to develop fully before extracing data such as temperature, pressure and velocity. Note that the extention is modeled as no-slip and adiabatic. The geometric domain for a dimpled channel is presented in Figure 3.7.

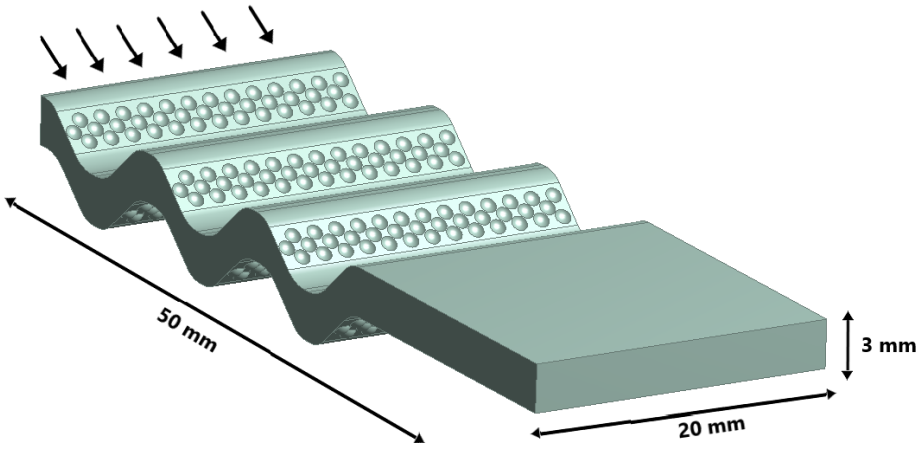

Figure 3.7 – Geometric domain for the singular heat exchanger channel study.

Boundary conditions, selection of turbulence model and meshing methodology was done according to section 3.1.

The mesh had 8.9 million elements including the inflation layer, with 4.8 million being tetrahedral and 4.1 million being rectangular. The volume of the domain was 3360 mm^3 which results in a cell density of 2650 $cells/mm^3$. The cell density is smaller compared to the study in section 3.2, however the resolution around the dimples is unchanged. The decrease in cell density is a result of the singular channel consisting mostly of bulk flow in the center of the channel, where cell density is less important. The cell resolution around the boundary layers close to the wall is equivalent to the previous study involving dimples surfaces. The geometry is slightly more complex in this study compared to section 3.2 which contained a flat surface with dimples. This study features a corrugated channel which requires a longer domain to allow the flow profile to develop fully, this is the reason for the increase in domain size, as compared to the study in section 3.2. Figure 3.8 shows the mesh for the singular channel.

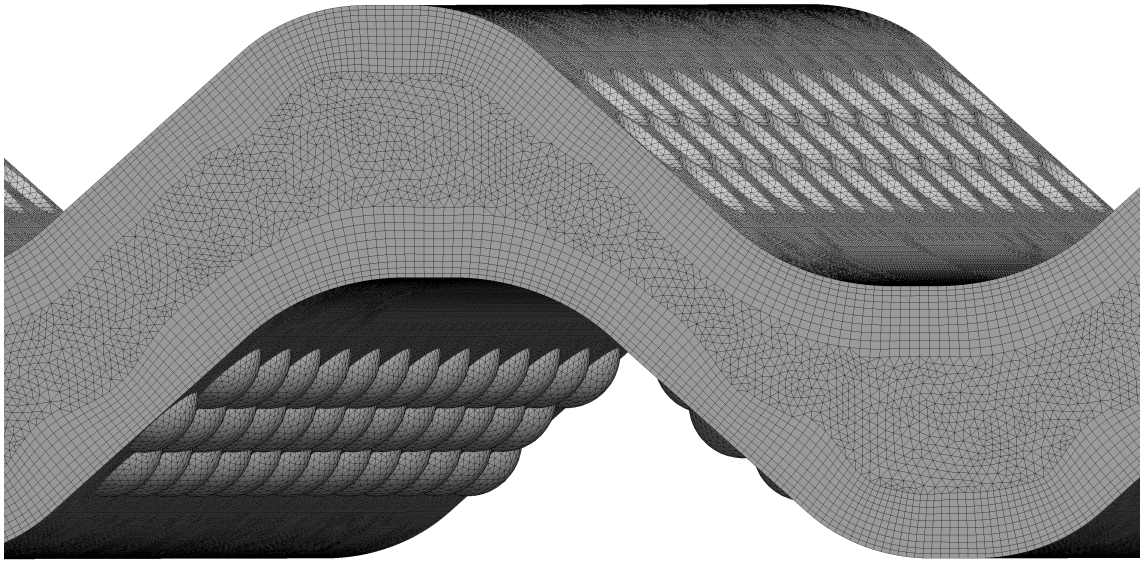

Figure 3.8 – Dimpled single heat exchanger channel.

The inflation layer can be seen in Figure 3.8 and allow for high resolution around the dimples. The mesh is structured and of good quality without a single element having a skewness above 0.9. The solver was set to steady state with a the residual target of 0.00005 residuals. Root square mean (RSM) was applied with a maximum 500 iterations if the convergence criteria was not met.

3.3.1 Position

The dimples can be placed at different points throughout the channel. Without considering the production difficulty of pressing the heat exchanger plate with dimples, the position of dimples can affect the pressure drop and thermal performance of the plate. This study is therefore dedicated to investigating where the dimples should be placed for optimal performance. Several possible positions are available, on the flanks of the indulations and on the apex at the top of the channel curvature. Additionally, one could consider that the dimples should be placed with alternating direction regarding obtruding and protruding dimples.

After considering possible arrangements, the scope was narrowed down to 4 geometries to be investigated, which are named: Apex-position all down, Apex-position alternating, Flank-position and Flat. Illustrations of all four geometries can be found on the next page, in Figure 3.9.

As can be seen in Figure 3.9 there are four geometries that have dimples places at different positions throughout the channel. The first geometry has dimples, all facing the same direction, located at the apex of the channel. The second geometry has alternating protruing and obtrusive groups of dimples located at the apex of the channel. The third geometry has dimples located on the flanks of the channel and the fourth geometry is flat, without dimples. The fourth geometry will be used as a basecase to compare against.

The geometries will be evaluated in terms of heat transfer, pressure drop and thermal efficiency, equivalent to section 3.2.

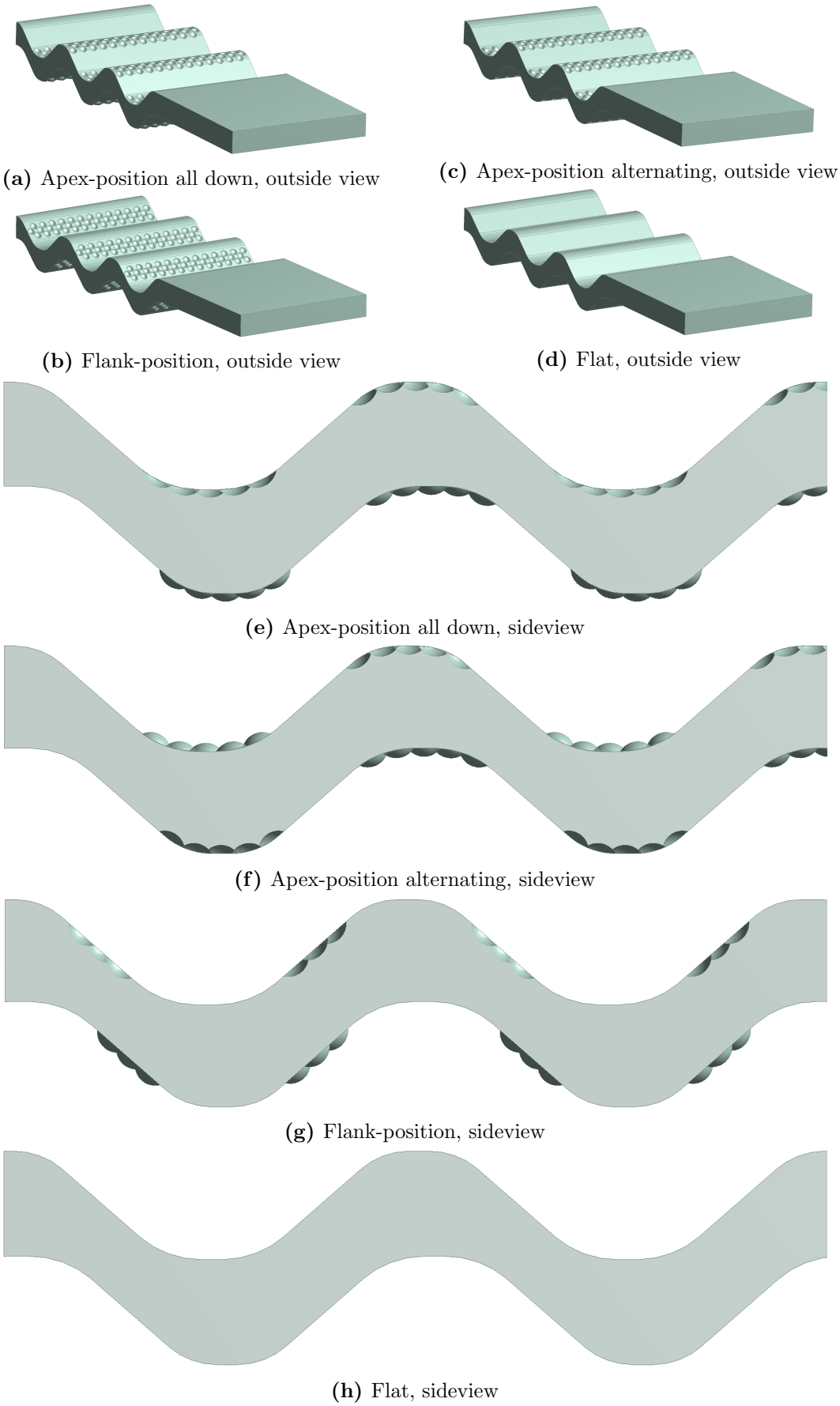

(a) Apex-position all down, outside view

(c) Apex-position alternating, outside view

(b) Flank-position, outside view

(d) Flat, outside view

(e) Apex-position all down, sideview

(f) Apex-position alternating, sideview

(g) Flank-position, sideview

(h) Flat, sideview

Figure 3.9 – Four channel geometries with dimples placed at different positions.

3.3.2 Near wall meshing sensitivity

Previous studies showed a trend that the heat transfer seemed to change with mesh resolution. The influence that mesh has on the model was therefore investigated by decreasing the element size and inflation layer element size at intervals and extracting quantities to obtain heat transfer, pressure drop and thermal efficiency. The goal is to determine the effect of mesh resolution, and to determine a sufficient resolution for this study. A dimpled channel geometry was used, more specifically the third geometry, Flank-position, in section 3.3.1 which was compared to a flat channel without dimples.

A central parameter when discussing mesh resolution is the distance from the wall measured in wall units, y^+ which is presented in equation 3.1

$$y^+ = \frac{u_\tau y}{\nu} \tag{3.1}$$

where u_τ is the friction velocity, y is the absolute distance from the wall and ν is the kinematic viscosity. Note that y^+ has a similar definition to the Reynolds number, with a length and velocity divided by a viscosity. This is no coincidence, as y^+ describes the relative importance of viscous and turbulent forces in the near-wall region, much like Reynolds number does for bulk flow. Different regions, or layers, near the wall are defined by the magnitude of y^+ which are presented below:

- **The viscous sublayer** $y^+ < 5$**:** In the viscous sublayer, viscous effects dominates the fluid flow, and turbulent forces are negligible. The velocity is linear.
- **The buffer layer** $5 < y^+ < 30$**:** The buffer region is a transition region between the viscosity-dominated and the turbulence-dominated regions. Viscous and turbulent forces are both present and creates a complex region were description of the velocity is not well defined.
- **The logarithmic area** $y^+ > 30$**:** The logarithmic region is dominated by turbulent forces and the viscous forces are negligible. The velocity profile varies slowly with logarithmic function known as the log law.

In the preprocessing stage of a CFD simulation, y^+ needs to be calculated to ensure that its in the desired range. Equation 3.1 can be rearranged to

$$y = \frac{y^+ \nu}{u_\tau} \tag{3.2}$$

where y is the height of the first mesh inflation layer. This equation can be used to calculate the required first inflation layer height for a certain $y+$, and will be used in the mesh sensitivity study. Table 3.2 describes the design points used in the mesh sensivity study.

Design point	First inflation layer height, y, [m]	y^+	Nusselt number Nu [-]	fanning friction factor C_f [-]	Thermal efficiency η [-]
DP 1	0.00215	-	-	-	-
DP 2	0.000129	-	-	-	-
DP 3	8.62E-5	-	-	-	-
DP 4	5.00E-5	-	-	-	-
DP 5	2.00E-5	-	-	-	-
DP 6	5.00E-6	-	-	-	-

Table 3.2 – Design points for investigating the mesh sensitivity.

3.4 Herringbone Pattern

This is the third and final case in the study of dimples in heat exchanger channels. This case will cover the implementation of dimples in a model of a real-life herringbone pattern used in one of Alfa Lavals heat exchanger products. A herringbone pattern consists of corrugated plates inclined at an angle, β, towards each other. The fluid flows through narrow openings between the plates, giving rise to high heat transfer and and high pressure drop. Compared to the first and second case, the flow structure inside the herringbone pattern is complex and chaotic, making a detailed analysis challenging.

The geometric domain for this study was a herringbone pattern with dimples added to the flanks of the channel. The geometric domain is presented in Figure 3.10.

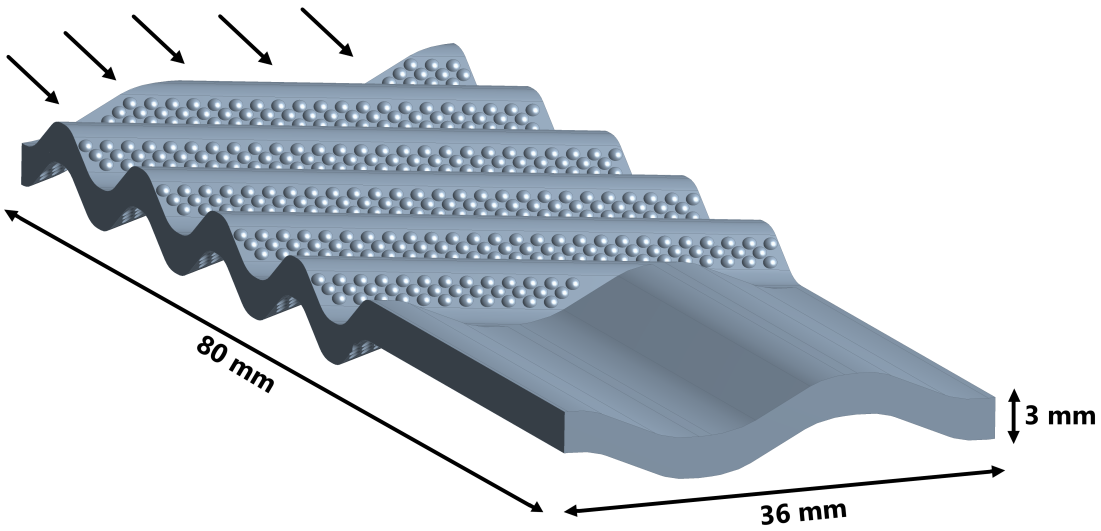

Figure 3.10 – Geometric domain for Herringbone pattern.

Figure 3.10 shows the herringbone pattern with dimensions and flow direction from back to front. Similar to previous studies, the extension to the right of the geometry was added to allow the flow profile to develop fully before extracting temperature, pressure and velocity. The extension was modeled as no-slip and adiabatic ensure that it does not interfere with the result of the simulation.

Boundary conditions, selection of turbulence model and meshing methodology was done according to section 3.2.

Note that the herringbone has undulations facing different directions between top and bottom. The undulations are inclined at a 60° angle, making the corrugation angle 60°. The corrugation angle is the main difference between the singular heat exchanger channel in case 2 and the herring bone pattern in case 3. To illustrate, a sideways view of the geometric domain with flow direction from left to right is presented in Figure 3.11.

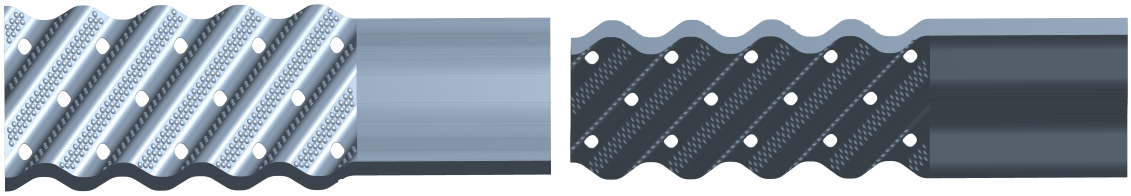

(a) Sideview, tilted downwards.

(b) Sideview, tilted upwards.

Figure 3.11 – Geometric domain for Herringbone pattern.

Notice that the undulations are angled at 60° between top and bottom. The holes that can be seen in Figure 3.11 are in fact contact points between the plates. The contact points provides a real challenge regarding meshing. A gradual decrease in height close to the edge of the contact point resulted in infinitely thin meshing elements, causing the meshing precedure to fail. This was solved by a custom mesh region around the contact points to allow mesh elements of a certain size. The mesh had a total of 19.8 million elements, with 6.7 million tetrahedral, 9.7 million wedges, 90 thousand pyramids and 3.3 million hexahedral elements. The volume of the domain was 8600 mm^3 which results in a cell density of 2302 $cells/mm^3$. The cell density is slightly lower than in section 3.3, but its not a big difference. The custom meshing regions around the contact points affect the mesh statistics, but improves the performance of the mesh overall.

3.4.1 Implementation of Dimples

Given that the implementation of dimples on the herringbone pattern is the final case of the report, all knowledge that has been acquired in the first and second case will be used. So far, the dimples has decreased thermal efficiency for the heat exchanger channel, a far from optimal result. The goal of this case was to use the results from the first and second case to give the dimples the best possible chance to succeed.

In the first case, Flow Structures on Dimpled Surfaces, the staggered arrangement of dimples was deemed superior. A staggered arrangement will therefore be used in this study. In the velocity study of the same case a Reynolds number of 6000-8000 was deemed most efficient. It is difficult to directly compare the Reynolds number for the first case and this case, due to the geometry in the herringbone pattern containing narrow channels and passages while the geometry in case 1 was a straight channel. The flow will be significantly more turbulent in the herringbone pattern compared to a straight channel as the velocity will accelerate in the narrow passages. This will affect the Reynolds number according to:

$$Re = \frac{D_h v \rho}{\mu} \tag{3.3}$$

It is therefore difficult to translate the results from the velocity study in case 1 to the herringbone pattern. The inlet velocity of 0.3 m/s, which corresponds to Reynolds number 4000 for a straight channel, will be used with in the herring bone case. However, one should keep in mind that the actual Reynolds number is likely larger than that due to the velocity increase described above.

In the second case, Singular heat exchanger channel, the position study revealed that the optimal position for dimples were at the flanks of the channel undulations. Therefore the dimples will be placed at the flanks of the undulations in the herringbone pattern aswell. The near wall mesh sensitivity study showed that y^+ should be kept around $y^+ = 1$ for sufficient meshing resolution around the dimples. Therefore the first inflation layer mesh height will be calculated to correspond to $y^+ = 1$.

When performing initial simulations, there was a trend in the convergence of the solution. The reported residuals showed an instationary, time dependent behavior, with significant fluctuations. The following figure shows the residuals reported after an initial steady state run.

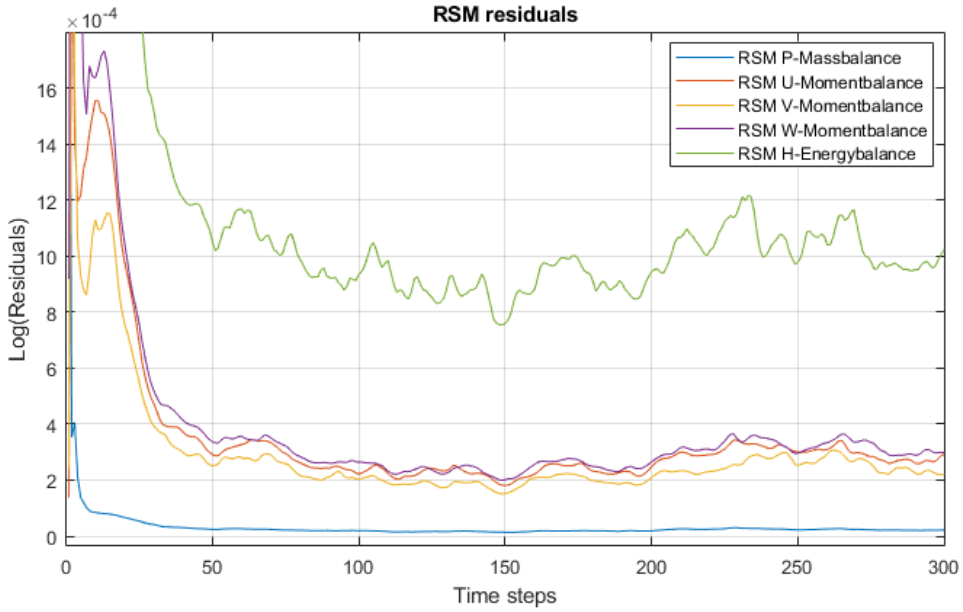

Figure 3.12 – RMS residuals for initial steady state simulation for a dimpled herringbone pattern.

Note that the moment, mass and heat residuals are fluctuating from iteration 50 and onwards. The heat balance is larger than optimal. Additionally, the residuals should preferably be reduced from the values in Figure 3.12, to increase convergence.

The trends in Figure 3.12 calls for a transient simulation that allow statistical sampling during a time period. The fluctuating residuals is a result of instationary flow behavior of the fluid, i.e that the solution is time dependent. Therefore the choice was made to switch from steady-state to a transient solver setup. A transient solution strategy revolves around taking incremental time steps throughout the domain, and performing iterations within each time step until a convergence criteria is reached. The result is a data set of monitor points from when the fluid enters the domain until the fluid leaves the domain, which allows postprocessing of the data to account for instationary behavior.

A transient simulation was setup with the goal of allowing the fluid to pass through the domain twice. The inlet velocity was 0.3 m/s and the domain is 85 mm long. It will therefore take $0.085/0.3 \approx 0.3$ *seconds* for the fluid to pass through the domain once. A second pass results in a total simulation time of 0.6 seconds. 2400 time steps was chosen between time 0 and 0.6 seconds, which gives 0.00025 seconds between each time step. Monitor points will be setup, taking samples of temperature, pressure and velocity at every time step. Figure 3.13 describes the setup of the transient simulation.

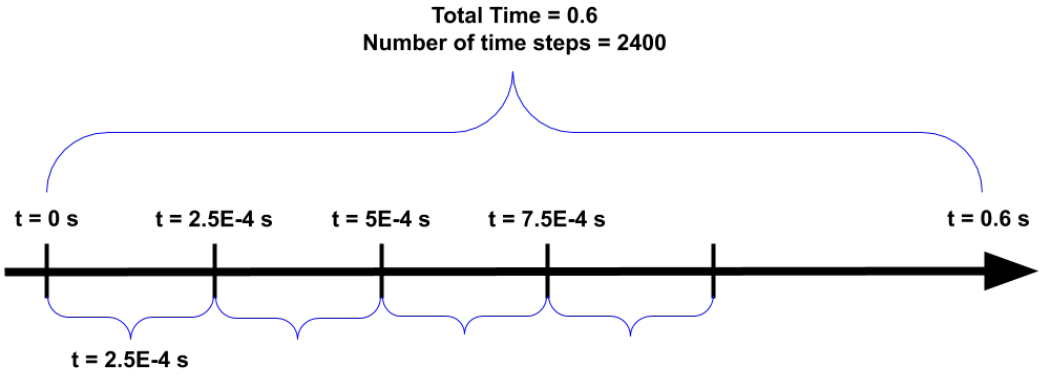

Figure 3.13 – Setup of the transient simulation with a total simulation time of 0.6 seconds and 2400 time steps.

Transient simulations produce a time dependent data set that can be post processed to draw conclusions from the data. By treating the data set as a signal with white noise, Fourier transform can be performed to determine amplitude and frequency of the signal.

Similar to previous studies, the dimpled herringbone pattern will be evaluated based on heat transfer, pressure drop and thermal efficiency against a herringbone pattern without dimples.

4 Result and Discussion

4.1 Flow structure on Dimpled Surfaces

4.1.1 Arrangement

To evaluate the performance of the staggered, in-line and flat arrangements three factors are considered: heat transfer, pressure drop and thermal efficiency. Heat transfer is represented by the Nusselt number, pressure drop by fanning friction factor and thermal efficiency by the thermal efficiency coefficient. After the simulation converged, data can be extracted and the results can be post processed. The mass-flow averaged temperature and area averaged pressure was extracted from each of the arrangements and are presented in Table 4.1 together with heat transfer area.

Arrangement	Heat tranfer area A_{HS} [mm]	Outlet temperature T_{Out} [°C]	Pressure drop Δp [Pa]
Staggered	116.2	23.01	14.68
In-line	116.2	22.97	14.2
Flat	106.8	22.56	11.51

Table 4.1 – Heat transfer area, massflow-averaged temperature and area averaged pressure drop from staggered, in-line and flat arrangement.

With the data from table 4.1 and using equations 2.3, 2.5 and 2.6, the Nusselt number, Fanning friction factor and thermal efficiency coefficient can be calculated. Table 4.2 presents the findings.

Arrangement	Nusselt number Nu [-]	Fanning friction factor C_f [-]	Thermal efficiency η [-]
Staggered	210	0.040	615.4
In-line	207	0.038	614.2
Flat	193	0.031	614.4
$^{\text{Staggered}}/_{\text{Flat}}$	**1.09**	**1.28**	**1.00**
$^{\text{In-line}}/_{\text{Flat}}$	**1.07**	**1.23**	**1.00**

Table 4.2 – Table with Nusselt number, Fanning friction factor and thermal efficiency coefficient for staggered, in-line and flat arrangement.

The results from table 4.2 shows several interesting things. Overall, dimpled arrangements has a greater heat transfer than without dimples, but with the penalty of increased pressure drop. This is intuitive due to the dimples protruding into the flow direction of the fluid near the surface of the wall, causing an altered flow path around the dimples. The dimples also provide increased heat transfer area which helps increase the heat transfer, see table 4.1.

In terms of arrangement, the staggered arrangement show a 9 % improvement in heat transfer compared to 7 % for the in-line arrangement. The pressure drop for the staggered case is greater with an 28 % increase compared to 23 % for in-line. The thermal efficiency proves to remain constant for both arrangements.

From these findings, the staggered arrangement performs the best based on heat transfer and the in-line arrangement performs the best based on pressure drop. Both arrangement follow the general relationship $\frac{Heat\ transfer}{pressure\ drop} = \frac{1}{3}$ which the thermal efficiency coefficient is based on. The relationship says that an increase in heat transfer would result in a three times increase in pressure drop. Therefore, the best arrangement is dependent on the application of the plate heat exchanger. If the goal is to maximize the heat transfer, the staggered arrangement is superior. However, if maintaining a low pressure drop is deemed important, the in-line arrangement performs better than the staggered.

Traditionally, the design of a plate heat exchanger is determined by the thermal and hydraulic load that is specified by the customer. A design parameter that is central to the design of a herringbone plate is the corrugation angle, β. An increase in β results in flow passages inclined at a steeper angle to the flow direction, causing enhanced heat transfer at the cost of pressure drop. It would seem that β depicts a similar trade-off in heat transfer vs pressure drop as the addition of dimples. The question then arises: Could adding dimples to the corrugated heat exchanger pattern be an additional parameter that should be considered when designing a plate heat exchanger? Could the design engineer choose to maintain a lower corrugation angle than what would normally be required, and add dimples to get a similar performance? Based on Table 4.2, it would seem that the answer is yes.

Flow structure analysis

The post-processing software in Ansys CFD allows the user to visually analyse scalar quantities through contour plots located throughout the domain. This can provide increased understanding to the flow structure around the dimples and its contribution to heat transfer enhancement. A thermal analysis can be performed based on Figure 4.1, which includes temperature contours of the domain for the staggered arrangement including a sideways view and a close up of a protruding and obtruding dimple.

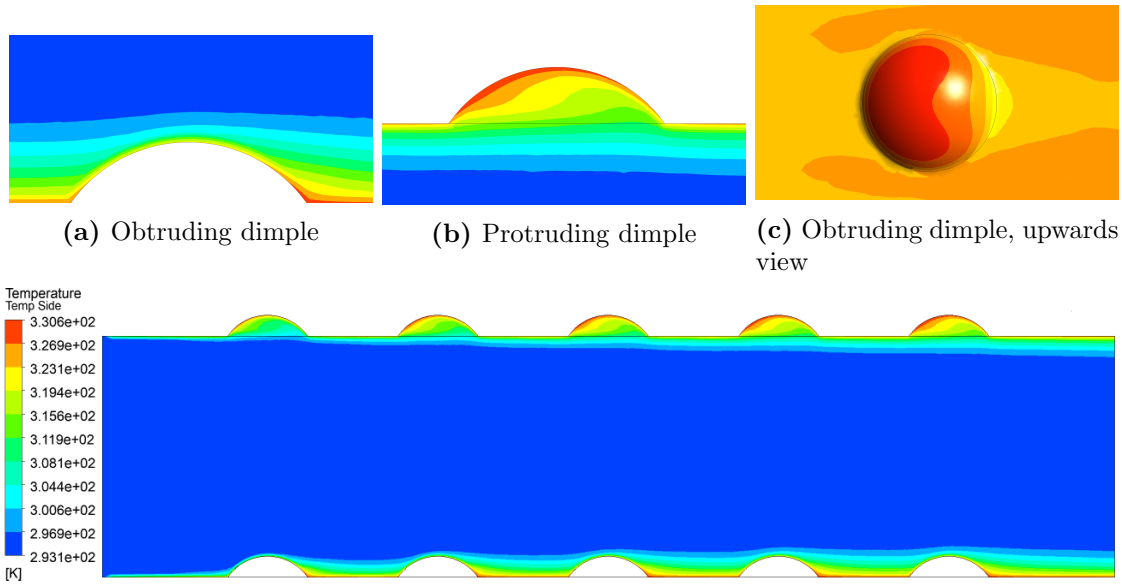

(a) Obtruding dimple **(b)** Protruding dimple **(c)** Obtruding dimple, upwards view

(d) Sideways view

Figure 4.1 – Temperature contour plot with flow direction from left to right.

Figure 4.1 shows the contribution that dimples have towards heat transfer enhancement. As can be seen in Figure 4.1 (d) the temperature is significantly higher in the wakes on the protruding side of each dimple and in the cavities of each dimple on the obtruding side. Figure 4.1 (b) and (c) show a close up view within the dimple cavity. The temperature reaches a maximum at the front half of the obtrusion and shows a minimum at the downstream rim. Figure 4.1 (a) shows a close up of a protruding dimple, which reveals a temperature maximum between adjacent protruding dimples. Bear in mind that a low temperature represents a region of high heat transfer, as this is where energy has been transported from the wall into the

fluid. The regions of high and low heat transfer can be explained by studying the velocity field. The velocity field is presented in Figure 4.2.

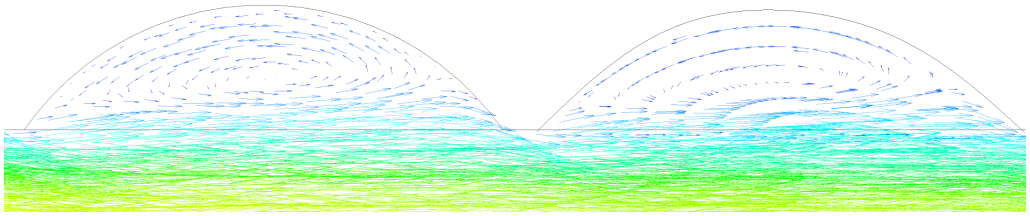

(a) Protruding dimple

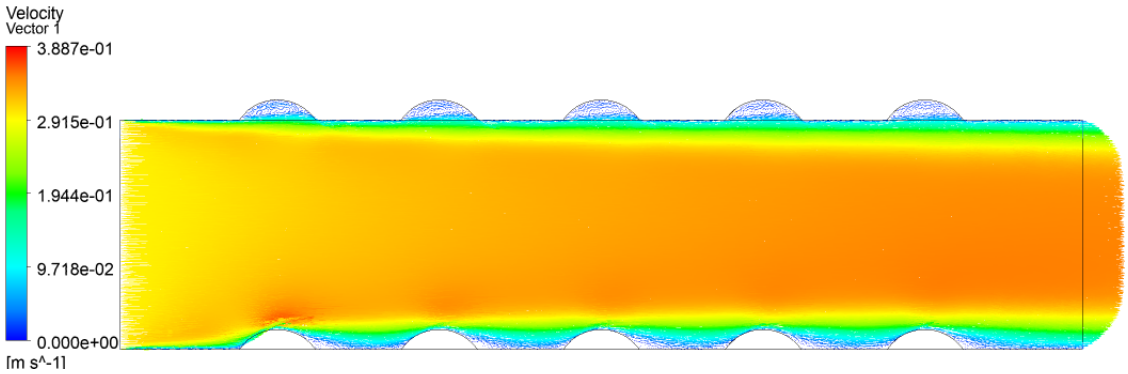

(b) Sideways view

Figure 4.2 – Velocity vector plot with flow direction from left to right.

Figure 4.2 (b) shows the velocity field of the domain. The velocity reaches its maximum in the middle of the domain and tends towards zero as it approaches the wall, as can be expected when no slip boundary conditions are applied. Close to the wall, as the flow moves parallel with a dimple, it hits the downstream edge of the dimple causing flow separation. The separated flow moves upwards in the dimple cavity approaching the apex of the dimple, and extends to the upstream edge to form a recirculation zone. The recirculation zone contains hot, slow moving media which is eventually remixed with the bulk of the flow at the upstream egde of the dimple. The recirculation zone in the dimple cavity can clearly be seen in Figure 4.2 (a).

The regions of low heat transfer in Figure 4.1 corresponds to the regions of low velocity in Figure 4.2. Specifically in the protruding dimple cavity, the heat transfer at the downstream rim is maximum due to the flow hitting this edge as parts of the flow is separated upwards into the dimple. The heat transfer is minimum in the front half of the dimple due to the recirculation zone trapping hot fluid, which prevents the driving force of heat transfer.

According to the theory in section 2.3, a prominent advantage of adding dimples is the formation of vortex structures which enhance mixing with the bulk of the flow. Although the present study is using a RANS-model to describe the turbulence, which does not capture local instantaneous velocity fields, an attempt is made to locate any coherent vorticities within the dimples. After experimenting with streamlines, the following structures was discovered, presented in Figure 4.3.

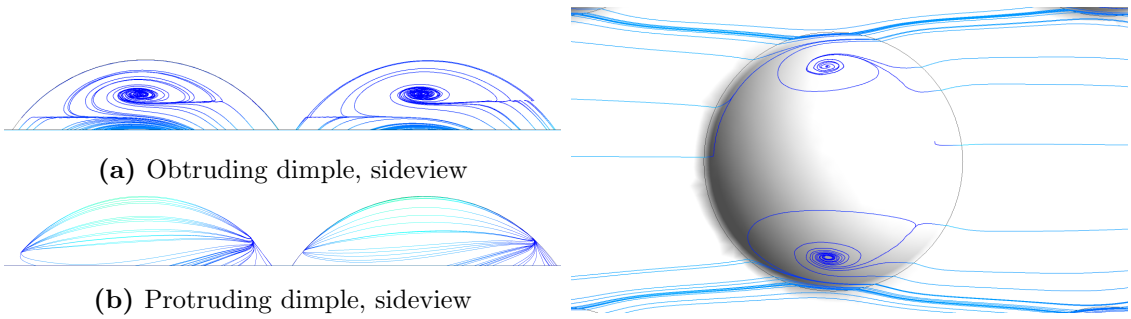

(a) Obtruding dimple, sideview

(b) Protruding dimple, sideview

(c) Obtruding dimple, upwards view

Figure 4.3 – Streamline revealing vortex-like structures inside the cavity of the dimples.

Figure 4.3 (a) and (c) shows two symmetric vortex-like structures on either side of the obtruding dimple. Figure 4.3 (b) shows the protruding side which reveal no abnormal structures other than the flow moving around the protruding dimple. The findings of vortexes in the cavities of dimples are not surprising, several other authors have described similar flow structures in previous studies using LES and DNS simulations (Chudnovsky and Kozlov 2006) (Elyyan 2008). However, what is surprising is that these structures were captured by the RANS model (SST k-ω). The fact that the RANS-model manages to capture these vortexes indicates that the vortexes are large-scale turbulent structures, located far up in the dissipative energy range, and would be resolved even better through LES or DNS simulations. Based on Figure 4.1 and 4.2, there is no evidence of the vortexes inducing enhanced mixing with the bulk flow, as no such phenomena can be identified in Figure 4.1. This is most likely a fault of the RANS-model, and shows limitations of the model compared to LES and DNS.

4.1.2 Reynolds Sweep

According to previous studies, see section 2.3, dimples act as turbulent generators that push the transition from laminar to turbulent flow. Naturally, dimples have different contributions to heat transfer and pressure drop at different Reynolds numbers and it is interesting to investigate this dependency. Therefore, Nusselt number and the Fanning friction factor was obtained at different velocities to investigate where dimples has the most effect, table 4.3 presents the findings.

Design point	Reynolds number Re_{norm} [-]	Heat transfer rate Q_{norm} [W]	Nusselt number Nu_{norm} [-]	Fanning friction factor $C_{f,norm}$ [-]	Thermal efficiency η_{norm} [-]
DP 1	2000	1.03	1.03	1.28	0.87
DP 2	4000	1.11	1.11	1.38	0.91
DP 3	6000	1.22	1.22	1.59	0.96
DP 4	8000	1.25	1.25	1.74	0.96
DP 5	10000	1.27	1.27	1.86	0.95
DP 6	12000	1.26	1.27	1.97	0.93
Average	-	**1.18**	**1.19**	**1.64**	**0.93**

Table 4.3 – Quantities measured during Reynolds sweep study for dimples in a staggered arrangement normalized with a flat case without dimples.

The Nusselt number and fanning friction factor in Table 4.3 can be presented in figures to further examine the trends, which is done in Figure 4.4.

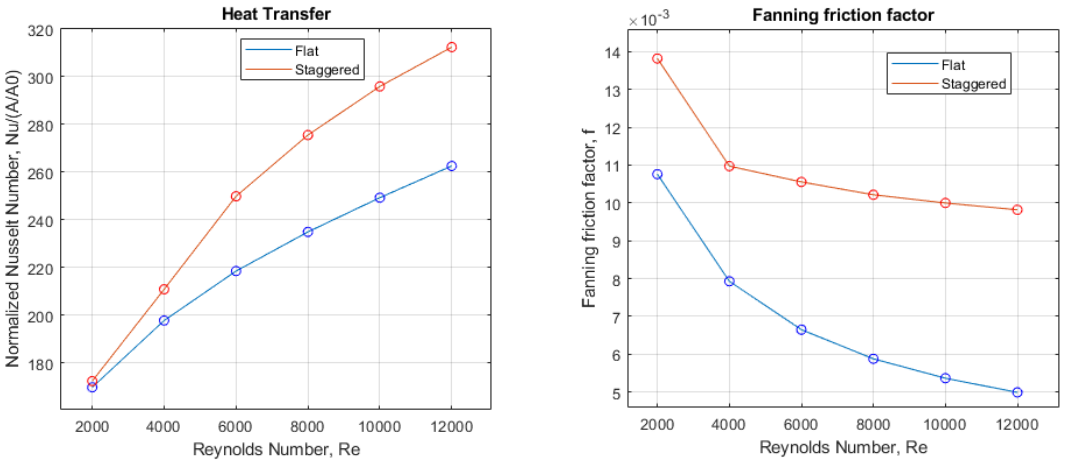

(a) **(b)**

Figure 4.4 – Heat transfer(left) and fanning friction factor(right) with dimples in a staggered arrangement (red line) and without dimples (blue line).

Figure 4.4 (a) shows that the heat transfer is enhanced by adding dimples. The dimpled model (red line) has a higher heat transfer than the undimpled model (blue line) at every design point in Figure 4.4 (a). As the Reynolds number decreases and laminar flow is approached, the effect of the dimples also decreases and the heat transfer of the dimpled channel approaches the heat transfer of the undimpled channel. As the Reynolds number increases, the heat transfer of the dimpled channel increases compared to the undimpled channel. The heat transfer at Reynolds number 12000 is 26 % larger for the dimpled channel compared to the undimpled channel.

Figure 4.4 (b) shows the fanning friction factor, with the red line being the dimpled model and the blue line being the undimpled model. Just like heat transfer, the friction factor is consistently larger for the dimpled channel with the difference increasing as the Reynolds number increases. The largest difference can be seen at high Reynolds number 12000 with the friction factor being almost double that of the undimpled channel.

The trade-off in heat transfer and pressure drop is depicted by the thermal efficiency coefficient, which can be seen in column 6 of Table 4.3 and in Figure 4.5.

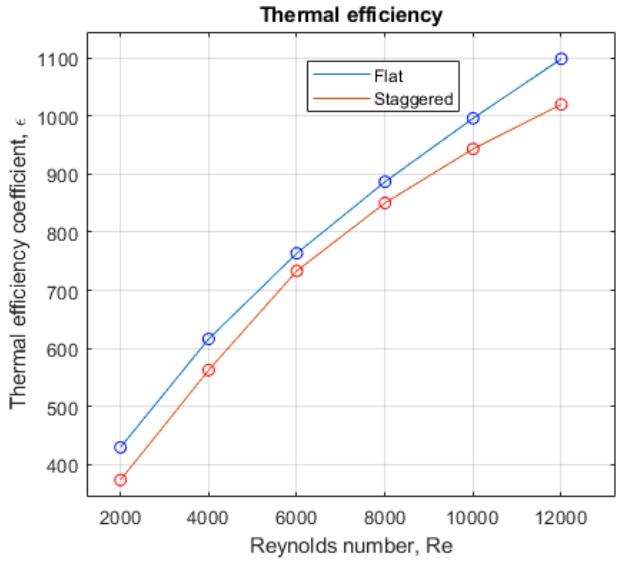

Figure 4.5 – Thermal efficiency with dimples in a staggered arrangement (red line) and without dimpled (blue line).

Figure 4.5 shows that the thermal efficiency is lower for the dimpled channel, which

is an unfortunate finding. The dimpled model preform best at Reynolds number 6000 and 8000 where the thermal efficiency is 96 % of the undimpled model, but its still a 4 % decrease in thermal efficiency. Even though the thermal efficiency has decreased by adding dimples, that does not mean that there is not a positive effect of adding dimples. Figure 4.4 (a) clearly shows that the heat transfer increases, up to 27 % at Reynolds number 10000, but the gain in heat transfer is counterfeited by an even larger pressure drop. If the implementation of dimples are to be considered, the positive heat transfer enhancement is largest between Reynolds number 6000 to 8000 due to the thermal efficiency being closest to the flat channel at these points.

4.2 Singular Heat exchanger Channel

4.2.1 Position

The four position where the dimples can be placed are evaluated by heat transfer, pressure drop and thermal performance. The goal is to determine if the position of the dimples affect the flow structure and thermal performance inside the heat exchanger channel, and if so, which effects are desirable and which are undesirable. Simulations were performed with dimples positioned at different places throughout the channel, according to Figure 3.9, keeping everything constant except the dimple position. Temperature and pressure drop were extraced at the outlet of the domain and the Nusselt number, fanning friction factor and thermal efficiency coefficient were calculated based on the extracted data. The results were normalized against the flat case and can be seen in Figure 4.6.

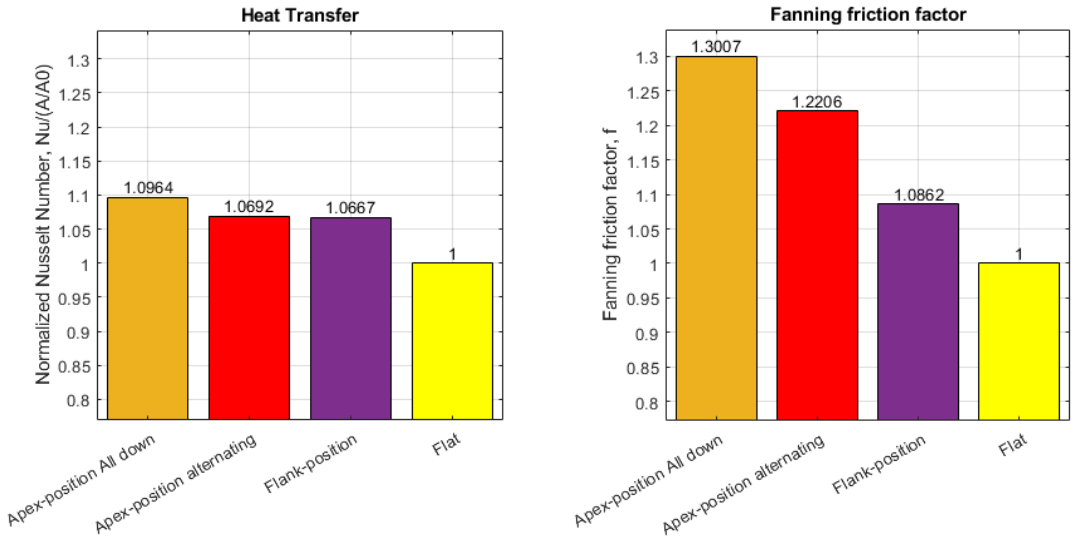

(a) **(b)**

Figure 4.6 – Nusselt number(left) and fanning friction factor(right) for dimples placed at different position normalized by a flat channel without dimples. Positions are: Apex-position All down(orange), Apex-position alternating(red), Flank-position(purple) and flat (yellow).

Figure 4.6 (a) shows that the heat transfer is enhanced for all dimples positions, with the largest increase (9.6 %) when the dimples are placed in Apex-position all facing downwards. The other two positions, Apex-position alternating and Flank-position, performs similarly to each other at an 6.9 % and 6.7 % heat transfer enhancement compared to a flat channel. Figure 4.6 (b) shows that the pressure drop also increases throughout all cases, with the Apex-position all down having the largest pressure

drop. The fanning friction factor is 22 % larger for Apex-position alternating and 8.6 % larger for Flank-position compared to the flat case. The thermal efficiency depicts the trade-off between heat transfer and pressure drop, and can be seen in Figure 4.7.

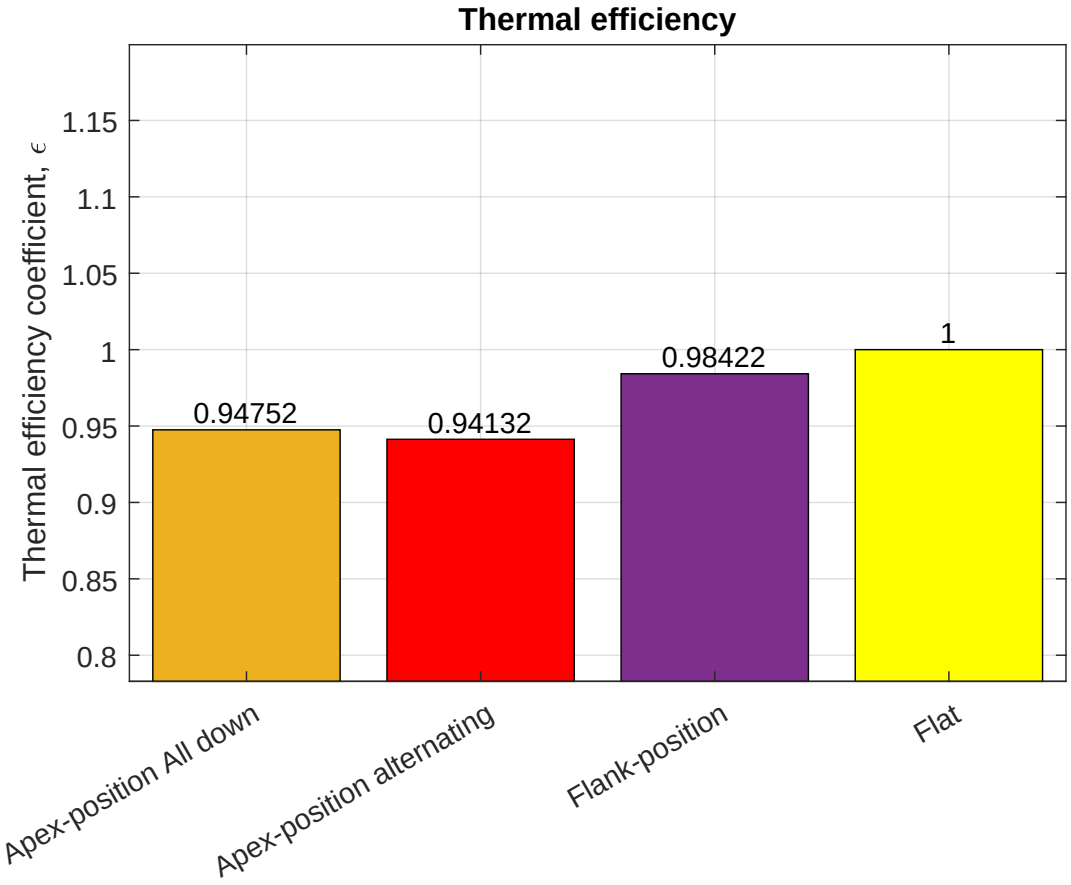

Figure 4.7 – Thermal efficiency for dimples placed at different positions normalized by a flat channel without dimples. Positions are: Apex-position All down(orange), Apex-position alternating(red), Flank-position(purple) and flat (yellow).

Figure 4.7 shows that the thermal efficiency is lower for all dimpled cases compared to a channel without dimples. Flank-position performs the best, but still has a 1.7 % lower thermal efficiency than a flat channel. This finding agrees with the findings in section 3.2, which also found that dimples give enhanced heat transfer, but the large increase in pressure drop makes the overall thermal efficiency go down. The position study shows that the best position for the dimples is in the Flank-position as the thermal efficiency largest for that case, however it is still lower than without dimples.

4.2.2 Near wall mesh sensitivity

To investigate the influence of mesh resolution on heat transfer, pressure drop and thermal efficiency the first inflation layer height was decreased at intervals. Temperature and pressure drop were extracted and converted into Nusselt number, Fanning friction factor and thermal efficiency. The wall distance measured in wall units, y^+, is also extracted from the simulation. y^+ is highly dependent on the geometry near the wall, and is gonna differ slightly between dimpled and undimpled channels even if the same inflation layer height was used. Table 4.4 shows the results for the dimpled channel and Table 4.5 shows the results for the flat channel without dimples.

Design point	First inflation layer height, y, [m]	y^+	Nusselt number Nu [-]	Fanning friction factor C_f [-]	Thermal efficiency η [-]
DP 1	0.00215	5.25	24	0.130	44.7
DP 2	0.000129	4.04	26	0.159	45.2
DP 3	8.62E-5	2.95	28	0.197	46.3
DP 4	5.00E-5	1.83	31	0.233	47.0
DP 5	2.00E-5	0.80	31	0.265	45.9
DP 6	5.00E-6	0.22	33	0.271	48.1

Table 4.4 – Design points dimpled singular channel for investigating the mesh sensitivity.

Design point	First inflation layer height, y, [m]	y^+	Nusselt number Nu [-]	Fanning friction factor C_f [-]	Thermal efficiency η [-]
DP 1	0.00215	5.52	20	0.118	41.4
DP 2	0.000129	4.07	24	0.156	48.2
DP 3	8.62E-5	3.22	27	0.180	48.0
DP 4	5.00E-5	2.08	29	0.215	48.0
DP 5	2.00E-5	0.87	29	0.247	46.7
DP 6	5.00E-6	0.22	29	0.249	45.6

Table 4.5 – Design points flat singular channel for investigating the mesh sensitivity.

To examine the trends of the mesh sensitivity study, the Nusselt number, Fanning friction factor and thermal efficiency is plotted against y^+. The result can be seen in Figure 4.8.

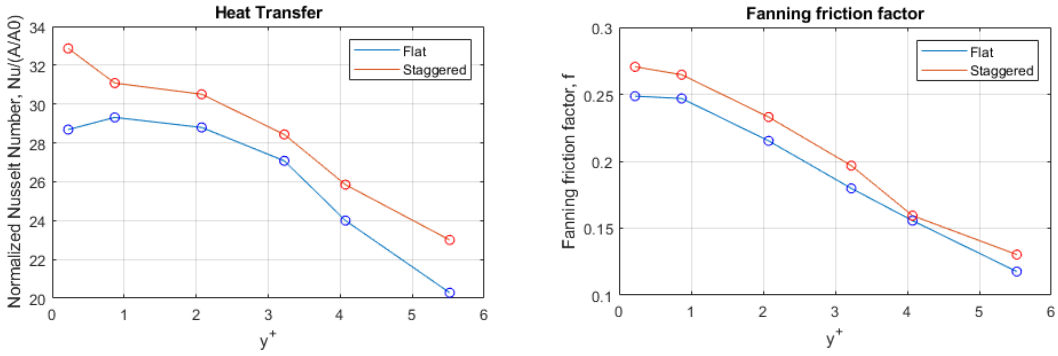

(a) **(b)**

Figure 4.8 – Nusselt number and Fanning friction factor plotted against the wall distance in wall units, y^+.

Figure 4.8 show clear trends between heat transfer, pressure drop and meshing resolution. Both heat transfer and pressure drop increase steadily with increasing meshing resolution, between $1 < y^+ < 5$. At $y^+ = 1$, the heat transfer curve flattens and seems to converge towards a value, only to diverge as y^+ approaches 0. This phenomenon is deemed to be a result of the RANS-model used ($SSTk-\omega$). $y^+ < 1$ results in very well resolved mesh close to the wall, much too fine for what the turbulence model is built to withstand. At such low y^+, to truly capture the effect of near wall flows, LES or DNS simulations are more suitable than RANS-models. Additionally, the curve for the dimpled and undimpled channel follow the same principal behavior which indicated that mesh resolution does not affect the dimpled channel differently than the undimpled channel.

In terms of magnitude, it is clear that both heat transfer and fanning friction factor are deeply dependent on meshing resolution. The heat transfer increases by 30 % and the fanning friction factor more than doubles at $y^+ = 1$ compared to $y^+ = 5$ for the dimpled channel, which is a worrying find. This means that the mesh resolution is a parameter which needs to be monitored closely when performing simulations in a heat exchanger channel, as an insufficient meshing resolution close to the wall can skew the results of the simulation.

The findings of Figure 4.8 shows that the heat transfer and pressure drop does indeed change with meshing resolution, as predicted in section 3.3.2. The model is valid above $y^+ > 1$, but fails below $y^+ < 1$ where the heat transfer diverges. With these results in mind, future simulations should be performed above $y^+ = 1$.

4.3 HerringBone Pattern

4.3.1 Implementation of dimples

The third and final case will cover the implementation of dimples in a herringbone pattern used in a real-life Alfa Laval heat exchanger product. The goal was to finalize the report by using results from previous cases to achieve the best possible performance and arrive at a recommendation for the usage of dimples in corrugated heat exchanger channels.

As discussed in section 3.4.1, initial simulations showed a tendency of instationary, time dependent flow behavior which motivated the switch from a steady state to a transient simulation setup. The residuals for an inital steady state simulation was presented in Figure 3.12 and showed fluctuations as well as large residuals values, indicating poor convergence. After the transient setup was adopted, the residuals provided different results. Figure 4.9 shows the residuals reported after transient setup, with the transient setup described in Figure 4.9.

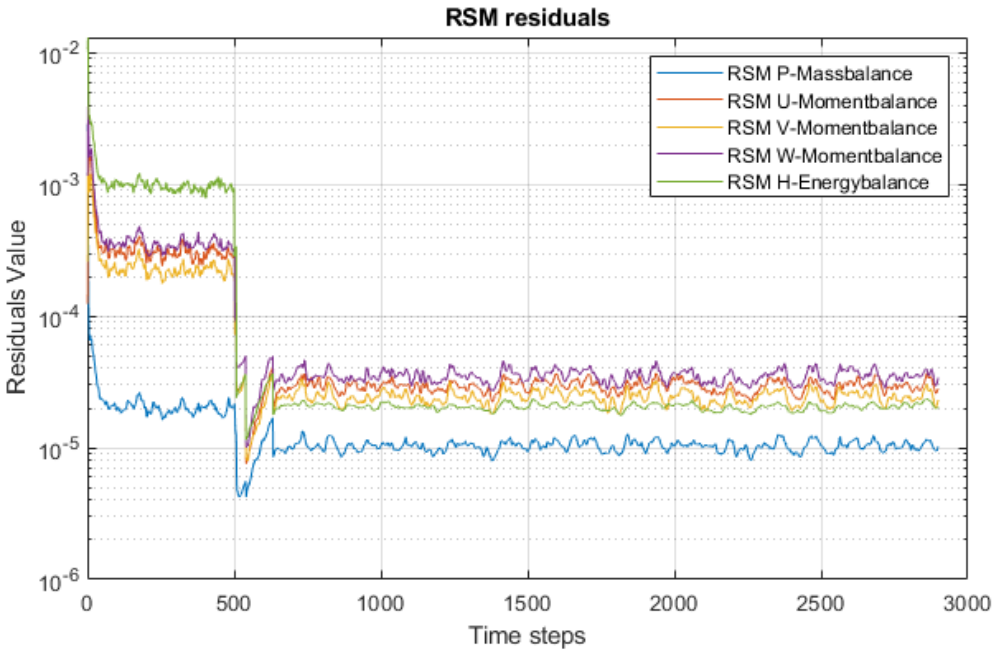

Figure 4.9 – RSM residuals reported for transient setup with steady state from time step 0-500 and transient from time step 500-2700.

As is evident in Figure 4.9, the residuals decrease when the transient setup is applied, at time step 500. This is a good thing, as the residuals depict the discrepancy in mass, moment and heat balance entering and leaving the domain and is therefore

a measure of convergence which is why small residuals are desirable. Compared to steady state, the transient setup showed increased convergence with the ability to analyze time dependent data with increased accuracy.

Data was extracted at two planes, an arbitrary plane in the middle of the domain and the outlet. Temperature, velocity and pressure drop was sampled at every time step, which results in a time dependent data set for pressure drop and temperature. This was done for both the dimpled and flat channel. A time averaged value can be obtained by averaging over every time step. To illustrate, Figure 4.10 shows time dependent pressure drop and temperature for the flat channel with the straight line showing the time averaged value.

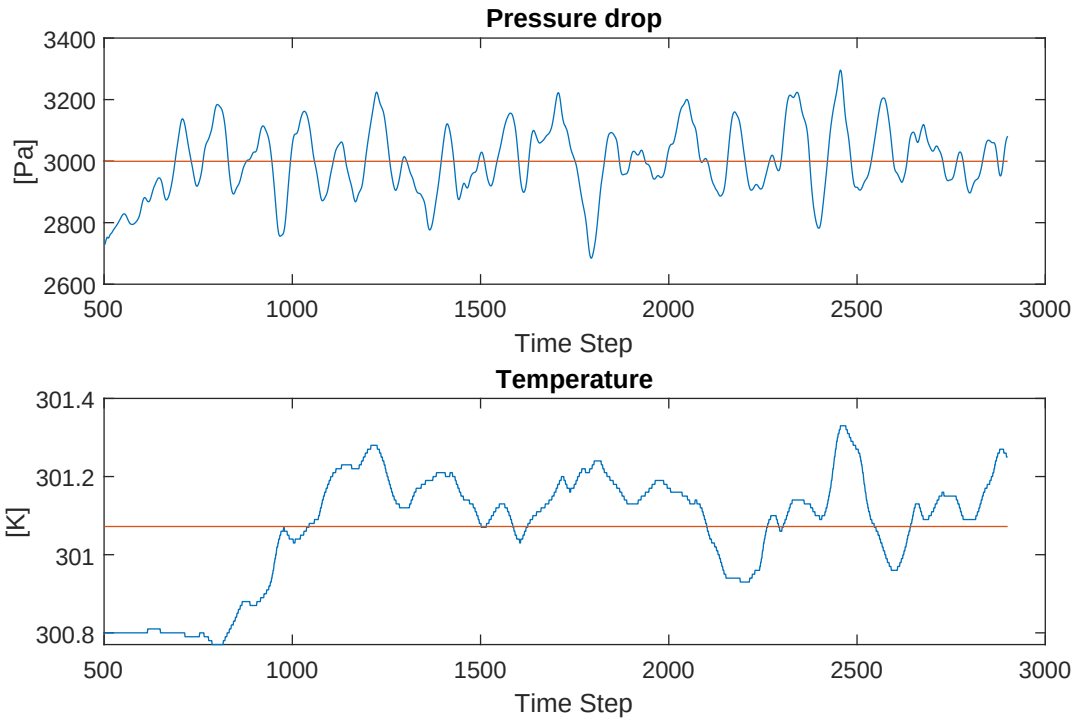

Figure 4.10 – Pressure drop signal (top), and temperature signal(bottom) at outlet with straight line representing the time average of the signal.

As can be seen in Figure 4.11, the pressure drop signal fluctuates between 2700 Pa and 3200 Pa, and the temperature fluctuates between 300.8 K and 301.3 K. This shows that the choice of transient simulation was justified, as the pressure drop and temperature for a steady state simulation could have been anywhere between the values above depending on where the simulation stops. A transient simulation allows for a time sampled average, which is statistically more reliable.

Fourier transform was applied to eliminate white noise and analyse the frequency of the sampled values. The result for pressure drop at outlet is presented in Figure 4.11 and Fourier transform for the other monitor points can be found in Appendix A.2, A.3 and A.4.

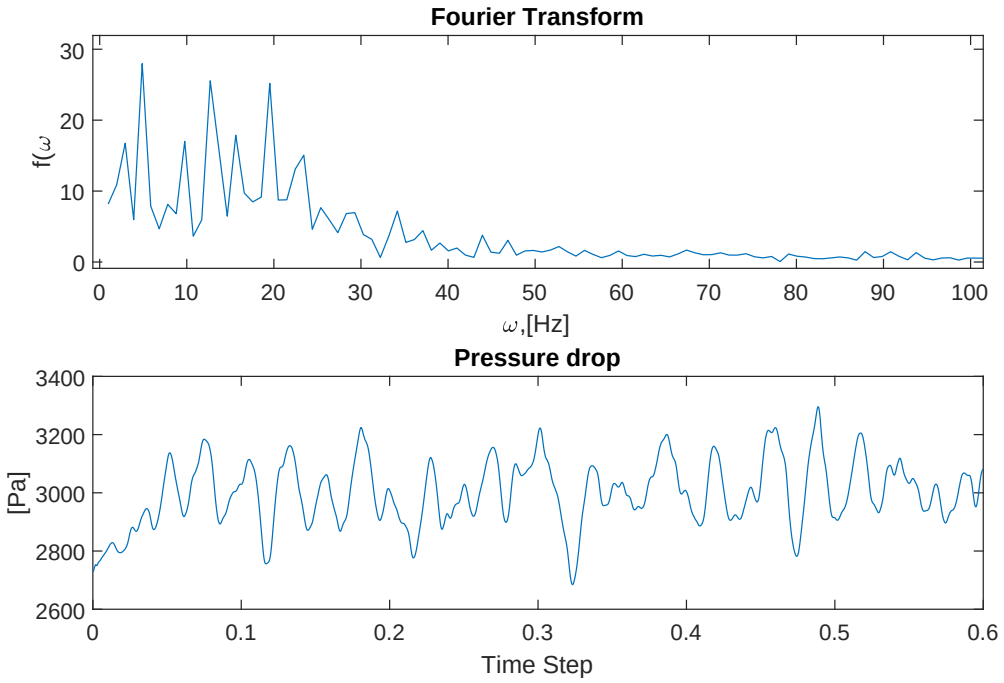

Figure 4.11 – Pressure drop signal (bottom), and Fourier transform of the pressure drop signal (top) at outlet.

Figure 4.11 shows the pressure drop signal in the bottom window and the fourier transform of the same signal in the top window. The Fourier transform shows that the data contain three main signals with different frequencies. The three signals corresponds to the three peaks that can be seen in the top window of Figure 4.11. The peaks have the frequency 5, 13 and 20 Hz which means that the signal oscillates at these frequencies. The frequency of the signal are believed to correspond to the flow structure inside the heat exchanger channel. The herringbone pattern creates vortexes and swirl flows which contribute to instationary flow behavior causing the extracted signals to oscillate. If the dimples have an effect on the flow structure inside the channel, creating vortexes and swirl flows, the frequency of the signals should clearly change compared to a herringbone pattern without dimples. To analyze whether the dimples has affected the frequency of the signal, the same procedure as above is performed for temperature, pressure and velocity on both the dimpled and flat channel. The figures in Appendix A.2, A.3 and A.4 shows the signal and

fourier transform of the signal. The figures does not show a clear frequency change between the dimpled and flat channel for any of the signals. The frequencies seem irregular and shows no visible trends which is why there is no conclusion to be drawn from the fourier analysis. This does not mean that the dimples have no effect, it simply means that the fourier analysis is not suitable for evaluating the effect of dimples.

To compare the data for dimpled and flat channel, data sets for temperature, pressure drop and velocity was extracted at the outlet and at an arbitrary plane called plane 3. The data sets were post processed to obtain time sampled averages which are presented in Table 4.6.

	Dimpled		**Flat**	
	Outlet	**Plane 3**	**Outlet**	**Plane 3**
Temperature T_{Out} [K]	301.7	301.4	301.1	300.6
Pressure drop Δp [Pa]	3056.6	620.5	2999.5	632.8
Velocity $\overline{v}$ [m/s]	0.43	0.50	0.44	0.53

Table 4.6 – Time sampled averages for temperature, pressure drop and velocity at plane 3 and the outlet for the dimpled and flat channel.

Table 4.6 shows that the temperature as well as pressure drop at the outlet is larger for the dimpled channel than for the flat channel, as expected. In plane 3, the temperature is also larger but the pressure drop is lower for the dimpled than for the flat channel. This is deemed to be an instability of the model, as the signal in plane 3 should ideally follow the trends of the outlet signal. The data in Table 4.6 was used to calculate Nusselt number, fanning friction factor and thermal efficiency through equations 2.3, 2.5 and 2.6. Table 4.7 presents the findings.

	Dimpled	Flat	$^{\text{Dimpled}}/_{\text{Flat}}$
Nusselt number Nu [-]	66	65	**1.02**
Fanning friction factor C_f [-]	2.87	2.81	**1.02**
Thermal efficiency η [-]	46.4	46.0	**1.01**

Table 4.7 – Table with Nusselt number, Fanning friction factor and thermal efficiency coefficient for dimpled and flat channel.

Following the trends of previous studies, the heat transfer and pressure drop is once again greater for the dimpled channel compared to the flat channel. The heat transfer is increased by 2 % and the friction factor has also increased by 2 % for dimpled channels compared to the flat channels. The thermal efficiency has proved to decrease for all previous studies, however when implemented on a herringbone pattern it increased by 1 %. This is an improvement of thermal efficiency, which has not been seen in previous studies. An explanation may be that the herringbone pattern already has a high pressure drop and large heat transfer, and implementing dimples therefore has insignificant effect. As Table 4.7 shows, there is barely any difference in thermal efficiency between the dimpled and flat channel. It is therefore possible that the margin of error is larger than the gain in thermal efficiency. Still, the simulation results from this study shows that adding dimples to a 60° herringbone pattern does increase the thermal efficiency marginally.

A 1 % increase in thermal efficiency is far from the promised increase in thermal efficiency. The cause might be an insufficient turbulence model which fails to capture key flow phenomena. The RANS-model used (SST k-ω) does not capture dynamic, instationary behavior which might lead to underprediction of the heat transfer in the channel.

4.4 LES simulation

The usage of dimples has now been investigated in detail using a RANS-model. Section 3.2, 3.3 and 4.3 has shown that the thermal efficiency decreases or marginally increases when dimpled are added, which is the opposite of the expected result.

To examine if an LES would show a different result than the RANS model, a LES simulation was performed for the singular heat exchanger channel. The simulation was performed with the same conditions as in section 3.3, but with the RANS-model exchanged for a LES. The expectation is that LES will capture the small-scale turbulent structures which influence the flow profile in the channel. Temperature and velocity of the LES simulations are presented below in Figures 4.12-4.15.

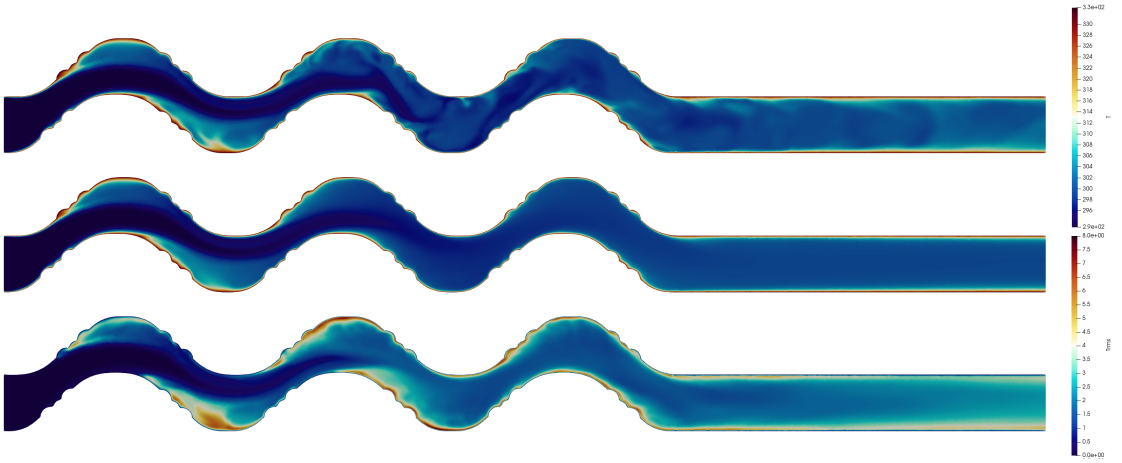

Figure 4.12 – Temperature in dimpled singular heat exchanger channel with an instantaneous profile (top) time averaged (middle) and rms-fluctuations (bottom).

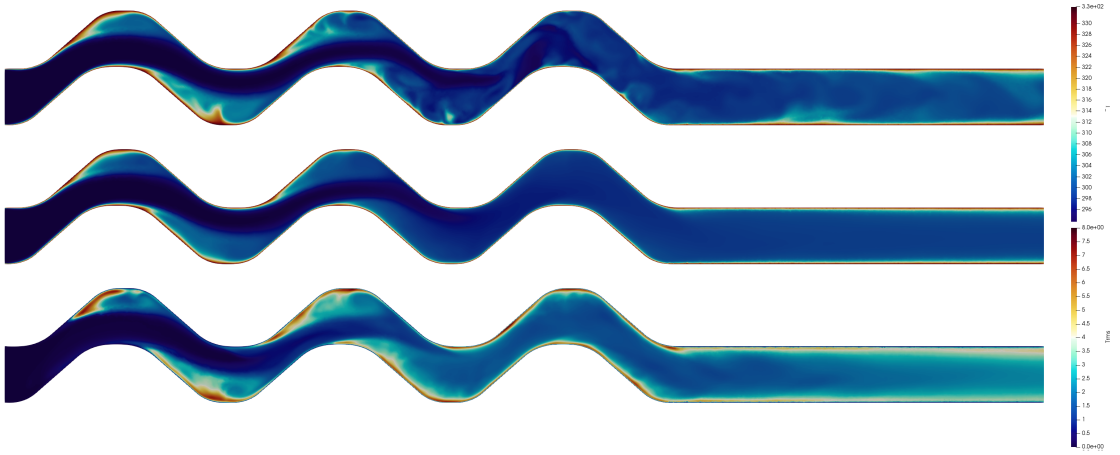

Figure 4.13 – Temperature in flat singular heat exchanger channel with an instantaneous profile (top) time averaged (middle) and rms-fluctuations (bottom).

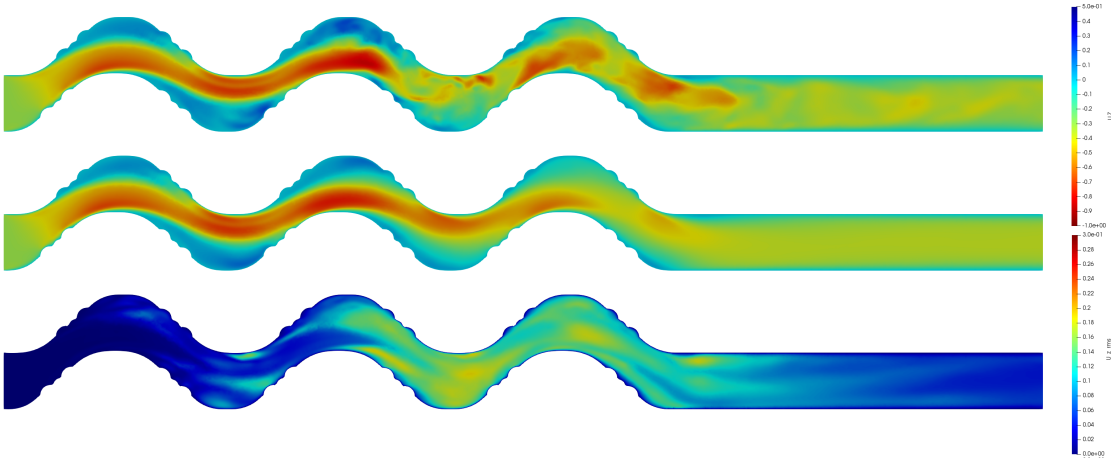

Figure 4.14 – Velocity in dimpled singular heat exchanger channel with an instantaneous profile (top) time averaged (middle) and rms-fluctuations (bottom).

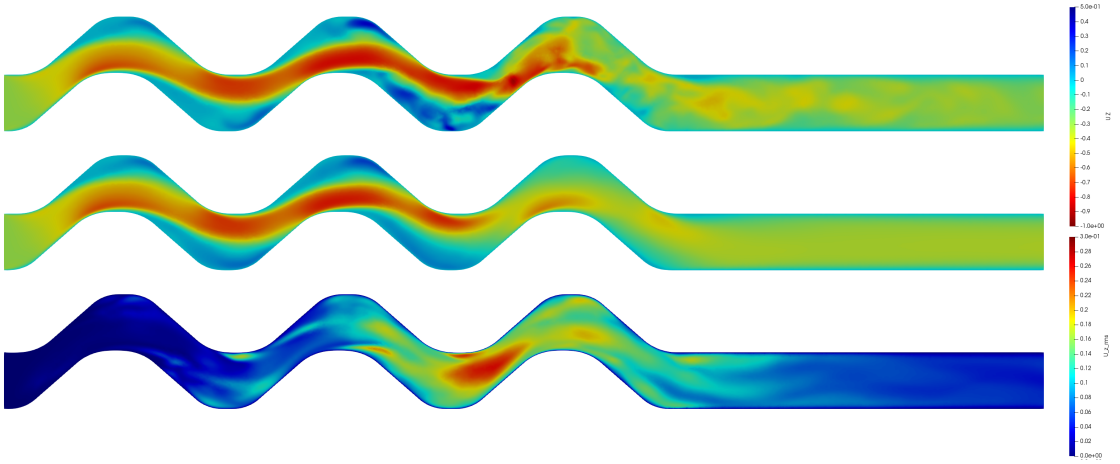

Figure 4.15 – Velocity in flat singular heat exchanger channel with an instantaneous profile (top) time averaged (middle) and rms-fluctuations (bottom).

The figures show several interesting phenomena. The rms-velocity fluctuations reveal significant vortexes forming from the dimple positions. These vortexes transport hot fluid from near the wall to the bulk of the flow which induces mixing. The effect of mixing can also be seen in the time averaged temperature, as the cold bulk of the fluid is dispersed sooner when dimples are added. The increased mixing disrupts the stream of cold fluid in bulk of the flow, which contributes to a more even temperature distribution. Additionally, the time averaged velocity show that the recirculation zones are diminished compared to the flat case which is a result of beneficial flow distribution when dimples are added.

None of these effects could be seen in the RANS-simulation which shows that RANS models are not suitable when investigating dimples. The complex flow structure with vortex formation and swirl flows which dimples provide requires description of small scale turbulent structures which RANS fails to do. For this application, LES is better suited.

Extraction of data from the LES-simulation showed that the outlet temperature increased by 2°C for the dimpled channel compared to the flat channel. This is a major improvement compared to an increase of 0.3 °C using a RANS-model in Section 3.3. The pressure drop increased by 3.4 % when adding dimples and using a LES model, which can be compared to the 8.6 % when using a RANS-model. Using these data, heat transfer, pressure drop and thermal efficiency can be calculated equivalent to section 3.3. Table 4.8 compares data from using a RANS-model in section 3.3 to LES.

	RANS			**LES**		
	Dimpled	Flat	$^{\text{Dimpled}}/_{\text{Flat}}$	Dimpled	Flat	$^{\text{Dimpled}}/_{\text{Flat}}$
Nusselt number Nu [-]	42.5	42.0	**1.01**	139.4	116.2	**1.20**
Fanning friction factor C_f [-]	0.23	0.21	**1.09**	0.30	0.29	**1.05**
Thermal efficiency η [-]	69.9	71.0	**0.98**	207.6	176.2	**1.18**

Table 4.8 – LES and RANS simulation showing Nusselt number, Fanning friction factor and thermal efficiency coefficient for the dimpled and flat channel.

Table 4.8 shows that there is a large discrepancy between RANS and LES when evaluating the performance of dimples. The RANS model fails to accurately describe the vortex formation, mixing and recirculation zones according to the discussion above, which causes the effect of dimples to go unnoticed in a RANS simulation.

These results show that dimples does infact increase the thermal performance of plate heat exchangers. The flow structure inside the channel in terms of vortex formation and mixing is affected greatly dimples, which has positive effects on the thermal performance of a plate. A secondary objective was to increase the understanding of flow structures inside plate heat exchanger channels. This has also been achieved as detailed descriptions of the flow has been developed, and phenomena such as vortex formation, recirculation zones and mixing has been investigated.

To summarize the findings of the report: The project started by investigating dimpled surfaces which showed that placing the dimples in a staggered arrangement was superior in terms of heat transfer and an in-line arrangement was superior in terms of pressure drop. A flow structure analysis revealed that the dimples contain hot, recirculating fluid which enhances mixing in the channel. Two symmetric vortex structures were found on either side the dimple cavity, which supports the fact that dimples provide additional turbulence through vortex formation. A study of the dependency between thermal efficiency and Reynolds number showed that the dimples perform best between reynolds number 6000-8000 but decreases the thermal efficiency compared to a flat surface.

Secondly, dimples were added to a singular heat exchanger channel with the goal of determining which position the dimpled should be placed in. The results show that the dimples should be placed on the flanks of the undulations for optimal performance, but once again the dimples were trumped by the flat channel which had a higher thermal efficiency. A mesh sensitivity study showed that mesh resolution near the wall influenced heat transfer and pressure drop significantly, and that the near wall meshing element should be kept above $y^+ > 1$ when using a RANS-model.

Thirdly dimples were implemented on a herringbone pattern. A transient simulation setup was adopted which increases statistical accuracy. A fourier transform was perform but yielded no visible frequency trends which deemed fourier transform unsuitable for this type of study. Thermal efficiency increased by 1 % when dimples were added, which was not enough to recommend an implementation in Alfa Lavals heat exchanger.

An LES simulation on the sinuglar heat exchanger channel was performed which yielded a 18% increase in thermal efficiency. Vortex formation, enhanced mixing and reduction of recirculation zones were observed when dimples were added.

The results of this paper show that dimples does increase the thermal performance of plate heat exchangers, but more importantly proves the importance of using the correct turbulence model for a given problem. The flow dynamics in a plate heat exchanger channel is complex, and the averaged quantities of a RANS-model is not sufficient for accurate description of the velocity field.

5 Conclusion

In this project, the objective was to investigate if dimpled geometries can increase the performance of plate heat exchangers.

The investigation has shown mixed results. Computational Fluid Dynamic Simulations using a RANS model has shown that the thermal efficiency tends to decrease when dimpled are added to a flat channel. The dimples were shown to have limited effect when added to a herringbone pattern due to the high heat transfer and large pressure drop already present in the original pattern.

More advanced LES simulations on a single heat exchanger channel showed that the RANS model is insufficient in its description of turbulent structures. LES proved that the thermal efficiency does in fact increase when dimples are added, due to enhanced mixing, formation of vortexes and reduction of recirculation zones inside the channel. As LES simulations have not been performed on a herringbone pattern, the effect of dimples on such a pattern is still uncertain. Without experimental data, it is difficult to draw explicit conclusions from the study connected to reality, as the model data need to be validated against laboratory trials.

The project has also shown that performing Computational Fluid Dynamic simulations of heat exchanger channels is challenging, due to complex and dynamic flow structures located inside the channel. For most R&D applications, RANS-models does not provide the necessary resolution to accurately describe the velocity profile. LES captures many of the desired structures, but is computationally more expensive than RANS resulting in a need for purpose-built computers with high computational capacity.

Recommendation for Alfa Laval: Based on the results of this paper, the most advanced simulation has shown that dimples increases the thermal performance of plate heat exchanger.

6 Future Work

In future, there are some additional elements that could be expanded upon.

First of all, the data extracted from the model could be validated through laboratory trials. This would allow model calibration which would ensure that the models describe reality. Future models could also contain conjugate heat transfer between a hot and cold stream instead of having a fixed heat transfer coefficient at the wall. This is how a real plate heat exchanger operates which could further approach reality.

Because of time and limited access to computational power, LES simulation of a herringbone pattern was never done in this report. This could be expanded in the future.

Given that this report is contained a strictly thermal analysis, production difficulties and mechanical strength is another factor which has not been investigated.

If dimples prove to be successful in future simulations, an economical analysis could also be performed to calculate the cost of pressing the dimples versus the savings that they provide.

References

Alfa Laval Corporate AB. (2020). *Technologies to trust*. URL: https://www.alfalaval.com/about-us/our-company/. (accessed: 31.05.2020).

Ansys Inc. (2020). *Ansys CFX 2019 R3 Manual*. URL: https://ansyshelp.ansys.com/account/secured?returnurl=/Views/Secured/prod_page.html?pn=CFX&prodver=19.5&lang=en. (accessed: 31.05.2020).

Banekar, Yogesh Dilip, Shashank Ram Bhegade, and Mayur Vasant Sandbhor (2015). "Dimple tube heat exchanger". In: *International Journal of Science, Engineering and Technology Research (IJSETR)* 4 (5), pp. 1632–1635.

Chudnovsky, Yaroslav and Aleksandr Kozlov (2006). "Developement and Field Trial of Dimpled-Tube Technology for Chemical Industry Process Heaters". In: *Gas Technology Institute*. DOI: https://doi.org/10.2172/894062.

Elyyan, Mohammad A. (2008). "Heat Transfer Augmentation Surfaces Using Modified Dimples/Protrusions". In: *European Fluids Engineering Summer Meeting* 1, pp. 1201–1211. DOI: https://doi.org/10.1115/FEDSM2006-98113.

Ferhat, Rabia et al. (2019). "Thermal Performance of a Corrugated Wall With Artifical Roughness". In: *Journal of Heat Transfer* 141.2, pp. 084501-1–084501-8.

Giram, Dhananjay R. and A.M. Patil (2013). "Experimental Theoretical Analysis Of Heat Transfer Augmentation From Dimpled Surface". In: *Int. Journal of Engineering Research and Applications* 3 (5), pp. 19–23.

Livya, E., G. Anitha, and P. Valli (2015). "Aerodynamic Analysis of Dimple Effect on Aircraft Wing". In: *International Journal of Aerospace and Mechanical Engineering* 9.2, pp. 350–353.

Pope, Steven B. (2000). *Turbulent Flows*. Cambridge University Press. ISBN: 0 521 59125 2 (hc).

Prasath, M.S and S. Irish Angelin (2017). "Effects of Dimples on Aircraft Wing". In: *Global Research and Development Journal for Engineering* 2 (5), pp. 234–242.

Shah, R.K, E.C Subbarao, and R.A Mashelkar (1986). *Heat Transfer Equipment Design*. Hemisphere Publishing Corporation. ISBN: 0-89116-729-3.

Turnow, Johann, Valery Zhdanov, and Egon Hassel (2012). "Flow Structures and Heat Transfer on Dimpled Surfaces". In: *International Journal of Heat and Fluid Flow* 35, pp. 168–175. DOI: https://doi.org/10.1016/j.ijheatfluidflow.2012.01.002.

Wikipedia The Free Encyclopedia. (2020). *Transient Modeling*. URL: https://en.wikipedia.org/wiki/Transient_modelling. (accessed: 31.05.2020).

A Appendix

A.1 Finite Volume Method

The most common solution method used in CFD is the finite volume method. The finite volume method is a solution methodology used to evaluate partial differential equations by converting volume integrals to surface integrals using Gauss divergence theorem. First, the region of interest is divided into smaller subregions based on the mesh, which are called control volumes. The control volumes are finite volumes constructed inside each mesh element, and are depicted in Figure A.1.

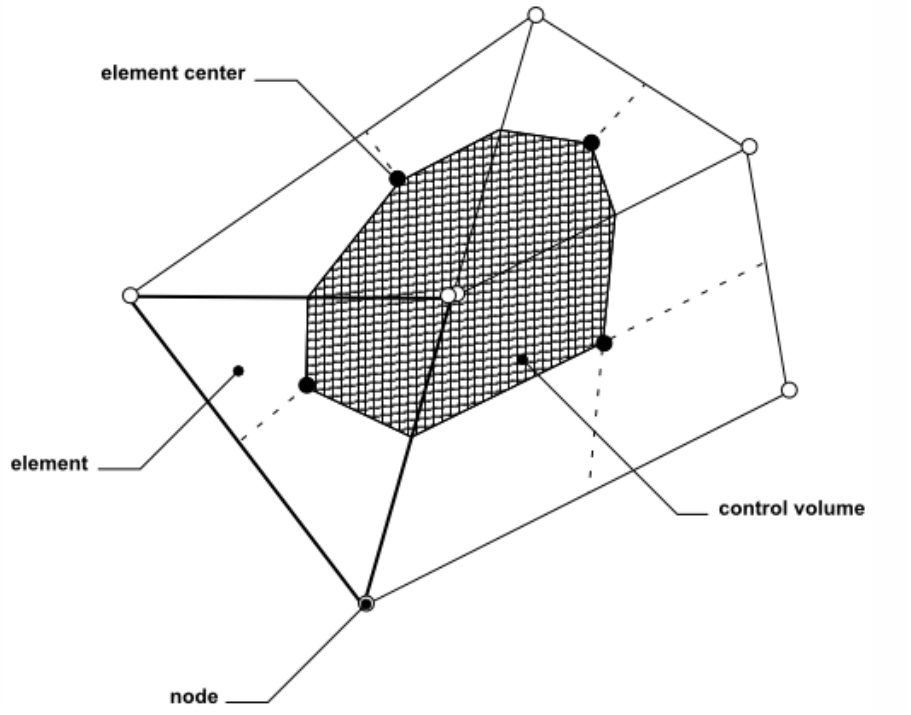

Figure A.1 – Definition of control volume inside a 2D mesh element.

The shaded area depicts the control volume. All solutions as well as fluid properties are stored at the nodes, which also serves as the mesh vertices. To demonstrate the finite volume method, consider the following partial differential equations for mass and momentum:

$$\frac{\partial \rho}{\partial t} + \frac{\partial}{\partial \boldsymbol{x_j}}(\rho \boldsymbol{v_j}) = 0 \tag{A.1}$$

$$\frac{\partial}{\partial t}(\rho \boldsymbol{v_i}) + \frac{\partial}{\partial \boldsymbol{x_j}}(\rho \boldsymbol{v_j} \boldsymbol{v_i}) = -\frac{\partial P}{\partial \boldsymbol{x_i}} + \frac{\partial}{\partial \boldsymbol{x_j}} \left(\mu_{eff} \left(\frac{\partial \boldsymbol{v_i}}{\partial \boldsymbol{x_i}} + \frac{\partial \boldsymbol{v_j}}{\partial \boldsymbol{x_j}} \right) \right) + S_{vi} \quad \text{(A.2)}$$

The partial differential equations are integrated over each control volume to create volume integrals. Gauss Divergence Theorem is applied to convert volume integrals containing divergence to surface integrals. Assuming that control volumes do not deform in time, time derivatives can be moved outside of the volume integrals, and equation A.1 and A.2 becomes:

$$\frac{d}{dt} \int_V \rho dV + \int_S \rho \boldsymbol{v_j} dn_j = 0 \quad \text{(A.3)}$$

$$\frac{d}{dt} \int_V \rho \boldsymbol{v_i} dV + \int_S \rho \boldsymbol{v_j} \boldsymbol{v_i} dn_j = -\int_S P dn_j + \int_S \mu_{eff} \left(\frac{\partial \boldsymbol{v_i}}{\partial \boldsymbol{x_j}} + \frac{\partial \boldsymbol{v_j}}{\partial \boldsymbol{x_i}} \right) dn_j + \int_V S_{v_i} dV \quad \text{(A.4)}$$

where S denotes surface regions of integration,V denotes volume regions of integration, and dn_j is the Cartesian components of the outward surface vector. The next step is to discretize the volume and surface integrals, which is illustrated in figure A.2.

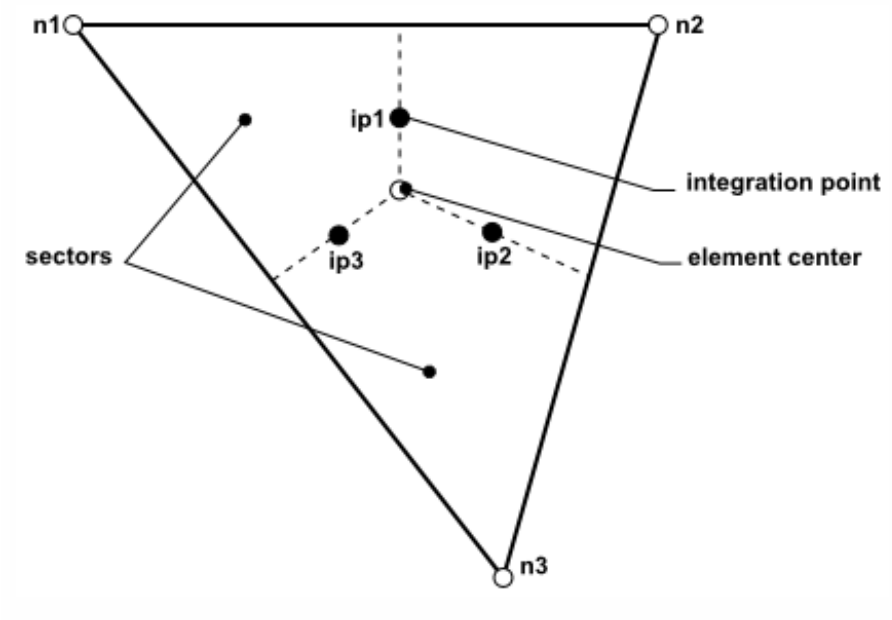

Figure A.2 – Mesh element illustrating discretization procedure.

The volume integrals are discretized within each element sector and shared to the control volume in which the sector belongs. Surface integrals are discretized at the

integration points, *ipn*, located at the center of each surface segment, and shared to adjacent control volumes. Surface integrals for adjacent control volumes are equal, due to them sharing a common edge. After the volume and surface integrals are discretized, the integral equations become:

$$V\left(\frac{\rho-\rho^0}{\Delta t}\right)+\sum_{ip}\dot{m}_{ip}=0 \tag{A.5}$$

$$\begin{aligned} V\left(\frac{\rho\boldsymbol{v_i}-\rho^0\boldsymbol{v_i^0}}{\Delta t}\right)+\sum_{ip}\dot{m}_{ip}\left(\boldsymbol{v_i}\right)_{ip}= \\ \sum_{ip}\left(P\Delta n_i\right)_{ip}+\sum_{ip}\left(\mu_{eff}\left(\frac{\partial\boldsymbol{v_i}}{\partial\boldsymbol{x_j}}+\frac{\partial\boldsymbol{v_j}}{\partial\boldsymbol{x_i}}\right)\Delta n_j\dot{m}_{ip}+\overline{S_{v_i}}V\right. \end{aligned} \tag{A.6}$$

Where $\dot{m}_{ip}=(\rho\boldsymbol{v_j}\Delta n_j)_{ip}$ and Δt is the time step. Equations A.5-A.6 are now discrete and can be solved for each control volume throughout the domain which will give approximated numerical values of the quantities v_i and v_j. The subscript *ip* denotes evaluation at an integral point and summations are done over all integral points of each control volume. Superscript ^{0} refers to an old time solution (Ansys Inc. 2020).

A.2 Fourier transform - Pressure drop

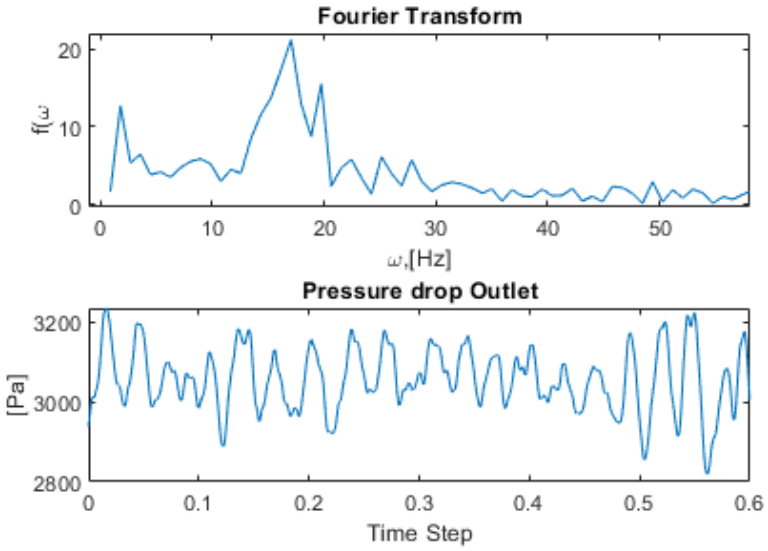

Figure A.3 – Dimpled

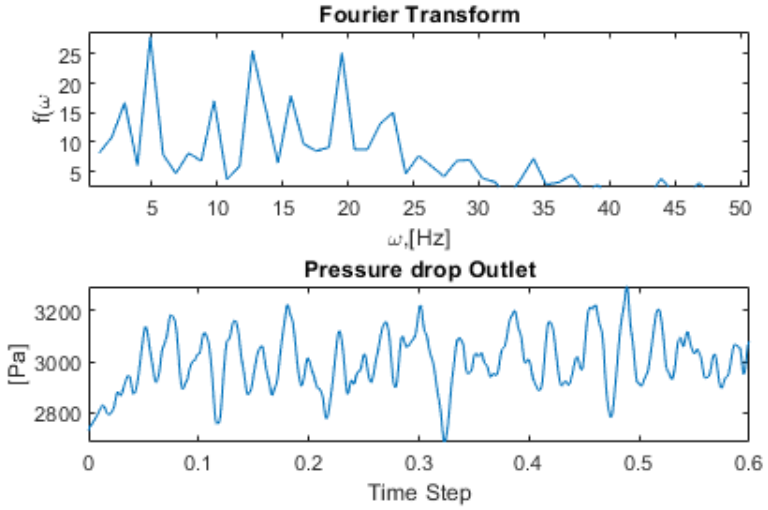

Figure A.4 – Flat

A.3 Fourier transform - Temperature

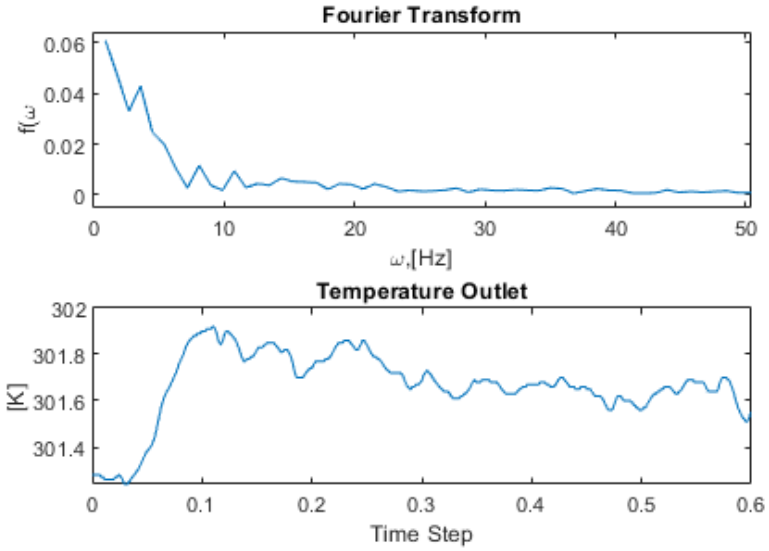

Figure A.5 – Dimpled

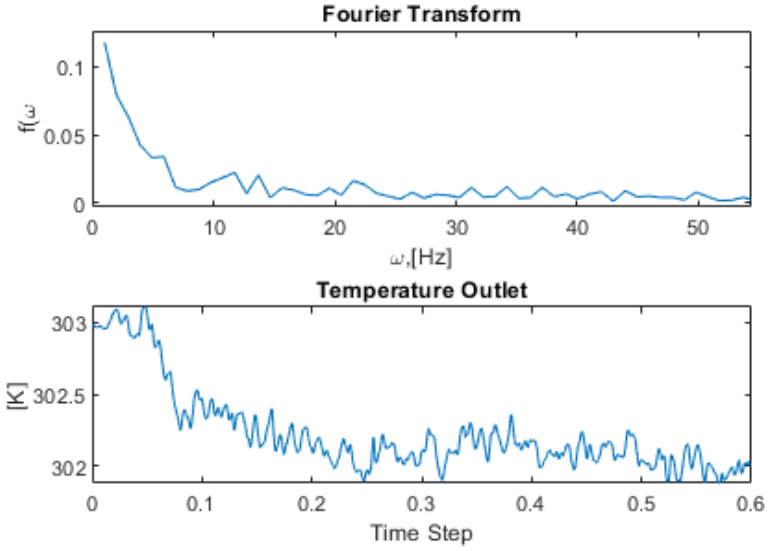

Figure A.6 – Flat

A.4 Fourier transform - Velocity

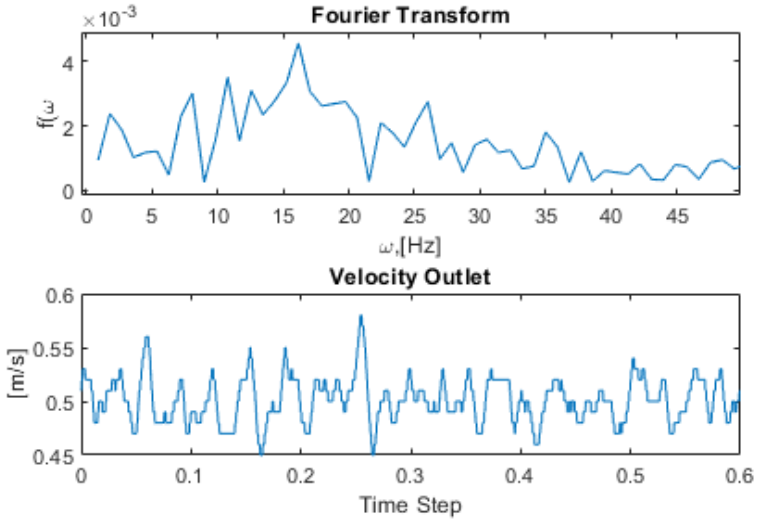

Figure A.7 – Dimpled

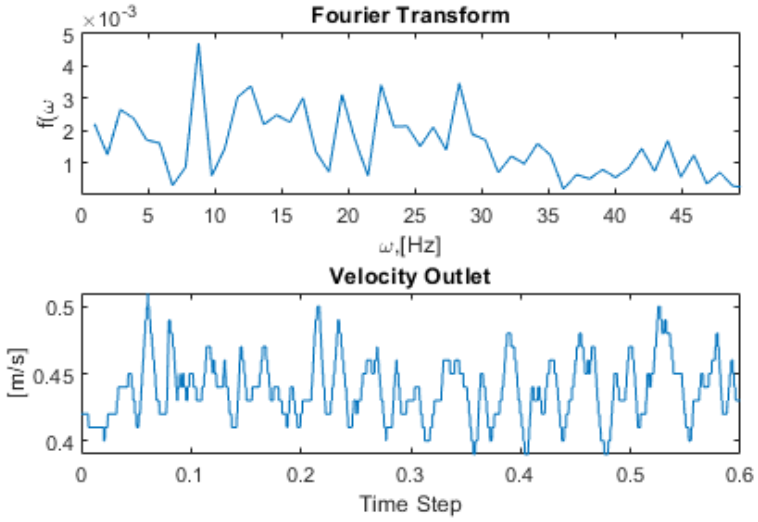

Figure A.8 – Flat